Journal of Materials Chemistry B

ROYAL SOCIETY OF CHEMISTRY

PAPER

View Article Online
View Journal | View Issue

Check for updates

Cite this: J. Mater. Chem. B, 2024, 12, 1096

Published on 02 Januari 2024. Downloaded on 19/07/2025 18:32:17.

# A potent multifunctional ZIF-8 nanoplatform developed for colorectal cancer therapy by triple-delivery of chemo/radio/targeted therapy agents†

Sonia Iranpour,[a] Ahmad Reza Bahrami,[ab] Mahdieh Dayyani,[c] Amir Sh. Saljooghi *[de] and Maryam M. Matin *[ae]

Received 30th October 2023,
Accepted 30th December 2023

DOI: 10.1039/d3tb02571c

rsc.li/materials-b

Background: Multimodal cancer therapy has garnered significant interest due to its ability to target tumor cells from various perspectives. The advancement of novel nano-delivery platforms represents a promising approach for improving treatment effectiveness while minimizing detrimental effects on healthy tissues. Methods: This study aimed to develop a multifunctional nano-delivery system capable of simultaneously delivering an anti-cancer drug, a radiosensitizer agent, and a targeting moiety (three-in-one) for the triple combination therapy of colorectal cancer (CRC). This unique nano-platform, called Apt-PEG-DOX/ZIF-8@GQD, encapsulated both doxorubicin (DOX) and graphene quantum dots (GQDs) within the zeolitic imidazolate framework-8 (ZIF-8). To enhance the safety and anti-cancer potential of the platform, heterobifunctional polyethylene glycol (PEG) and an epithelial cell adhesion molecule (EpCAM) aptamer were conjugated with the system, resulting in the formation of targeted Apt-PEG-DOX/ZIF-8@GQD NPs. The physical and chemical characteristics of Apt-PEG-DOX/ZIF-8@GQD were thoroughly examined, and its therapeutic efficacy was evaluated in combination with radiotherapy (RT) against both EpCAM-positive HT-29 and EpCAM-negative CHO cells. Furthermore, the potential of Apt-PEG-DOX/ZIF-8@GQD as a tumor-specific, radio-enhancing, non-toxic, and controllable delivery system for *in vivo* cancer treatment was explored using immunocompromised C57BL/6 mice bearing human HT-29 tumors. Results: The large surface area of ZIF-8 (1013 $m^2$ $g^{-1}$) enabled successful loading of DOX with an encapsulation efficiency of approximately ~90%. The synthesis of Apt-PEG-DOX/ZIF-8@GQD resulted in uniform particles with an average diameter of 100 nm. This targeted platform exhibited rapid decomposition under acidic conditions, facilitating an on-demand release of DOX after endosomal escape. *In vitro* experiments revealed that the biocompatible nano-platform induced selective toxicity in HT-29 cells by enhancing X-ray absorption. Moreover, *in vivo* experiments demonstrated that the therapeutic efficacy of Apt-PEG-ZIF-8/DOX@GQD against HT-29 tumors was enhanced through the synergistic effects of chemotherapy, radiotherapy, and targeted therapy, with minimal side effects. Conclusion: The combination of Apt-PEG-DOX/ZIF-8@GQD with RT as a multimodal therapy approach demonstrated promising potential for the targeted treatment of CRC and enhancing therapeutic effectiveness. The co-delivery of DOX and GQD using this nano-platform holds great promise for improving the outcome of CRC treatment.

## 1. Introduction

Colorectal cancer (CRC) stands as the third most prevalent malignancy and ranks second for cancer-associated deaths in both genders worldwide.[1,2] Extensive research has demonstrated that conventional cancer treatment options, including surgery, chemotherapy, and radiotherapy (RT) are primarily poor-response approaches, leading to adverse side effects with limited success rates.[3] For instance, in a small study on doxorubicin (DOX) as a traditional chemotherapeutic agent, no clinical benefit was noted among 12 CRC patients.[4] Moreover, cardiac oxidative stress and histological changes in the heart tissue have

[a] Department of Biology, Faculty of Science, Ferdowsi University of Mashhad, Mashhad, Iran. E-mail: matin@um.ac.ir
[b] Industrial Biotechnology Research Group, Institute of Biotechnology, Ferdowsi University of Mashhad, Mashhad, Iran
[c] Radiation Oncology Department, Reza Radiotherapy and Oncology Center, Mashhad, Iran
[d] Department of Chemistry, Faculty of Science, Ferdowsi University of Mashhad, Mashhad, Iran. E-mail: saljooghi@um.ac.ir
[e] Novel Diagnostics and Therapeutics Research Group, Institute of Biotechnology, Ferdowsi University of Mashhad, Mashhad, Iran

† Electronic supplementary information (ESI) available. See DOI: https://doi.org/10.1039/d3tb02571c



This journal is © The Royal Society of Chemistry 2024

Published on 02 Januari 2024. Downloaded on 19/07/2025 18:32:17.

been demonstrated after DOX treatment in rats with CRC.[5] These drawbacks have prompted great efforts for expanding treatment options and identifying novel therapeutic approaches. Multimodal cancer therapy has emerged as a new strategy, opening up new avenues for cancer treatment in recent years owing to its capacity to attack tumor cells from multiple angles.[6] Nanotechnology has made considerable contributions to the multimodal therapeutic strategy by introducing a wide variety of drug delivery systems (DDSs), which offer advantages to improve therapeutic responses. DDSs provide various benefits, including anti-cancer drug-carrying capacity, the capacity to be manipulated, the potential to combine with different treatment modalities, and ultimately increasing the efficacy of conventional treatments.[7] To achieve this aim, zeolitic imidazolate framework-8 (ZIF-8), which is one of the most well-studied subcategories of the metal organic framework (MOF) family, has recently garnered great attention as a nanocarrier in cancer research due to its highly porous structure for efficient anti-cancer drug loading, pH-controlled cargo release behavior, and the ability to incorporate/couple with several agents such as imaging tracers, targeting molecules, photoabsorbers, and radiosensitizer nanoparticles (NPs).[8,9] A radiosensitizer is an RT component that makes cancer cells more vulnerable to radiation, increases the lethal effect, decreases the radiation dose, and prevents damage to nearby healthy tissues.[10] With progress in nanomedicine, graphene quantum dots (GQDs) have been introduced as novel nano-radiosensitizers.[11] They belong to the family of carbon nanomaterials[12] and are well-known because of their intriguing properties such as low toxicity,[13] ultra-small size,[14] excellent biocompatibility,[15] strong fluorescence,[16] photothermal conversion capability,[17] and high X-ray absorption coefficients.[11] Due to the aforementioned facts, GQDs are frequently employed as nano-therapeutic agents in combination with photothermal therapy (PTT) and RT approaches. Recently, Liu and co-workers have reported a type of GQD (9T-GQD) to achieve the effect of photothermal conversion upon irradiation with a second near-infrared laser (NIR-II; 1064 nm, 1.0 W $cm^{-2}$). The temperature of the 9T-GQDs (0.2 mg $ml^{-1}$) rose to $\sim$49 °C under NIR-II laser irradiation, exhibiting a considerable photothermal conversion efficiency (33.45%).[18] In a study by Ruan *et al.*, the authors reported an increase in radiation energy deposition in the SW620 and HCT 116 human CRC cells treated with GQDs in combination with a low-energy γ-ray source (3 Gy).[11] This is mainly due to the overproduction of reactive oxygen species (ROS) and the synergistic effect of GQDs upon ionizing radiation.[19,20] Other investigations have demonstrated that MOFs are suitable for increasing the efficiency of PTT and RT. Recently, Tian *et al.* improved chemotherapy *via* designing a multifunctional platform based on DOX-ZIF-8/GQDs. They demonstrated that under 808 nm NIR radiation, the viability of 4T1 breast cancer cells treated with DOX-ZIF-8/GQDs was significantly reduced owing to the synergistic effects of chemotherapy and PTT.[21] Lan *et al.* conjugated hafnium (Hf), a powerful X-ray-absorbing component, with MOFs and evaluated the efficacy of RT in a mouse model of colon cancer treated with Hf-based MOFs.[22] In another work, MOF nanocarriers were developed as an intelligent nano-delivery system to load DOX and gold nano-radiosensitizers for combined chemo-radiotherapy. The *in vitro* and *in vivo* results of glioblastoma tumor treatment showed that, DOX@MOF-Au-PEG almost completely suppressed the U87MG tumors in combination with RT (inhibition ratio was up to 89%).[23] Moreover, Zhou *et al.* demonstrated improved treatment outcomes for esophageal cancer through the combination of UiO-66-$NH_2$(Hf) and RT both *in vitro* and *in vivo*.[24]

The effectiveness of DDSs can be increased *via* selective recognition of cancer cells in the tumor microenvironment (TME), known as active targeting, leading to enhanced local concentration around or within the tumor cells. In this context, critical features of cancer cell receptors including expression profiles, density, uniformity, and distribution patterns need to be evaluated carefully, and also compared with those in normal cells.[7] The most important aspects of active targeting include reducing off-target side effects, minimizing the likelihood of damage to healthy cells and optimizing the therapeutic outcome.[25] Among the classical targets, the epithelial cell adhesion molecule (EpCAM; CD326), a cell surface receptor, which is mostly overexpressed in the rectal cancer cells compared with adjacent healthy tissues, is a good candidate for CRC targeted therapy.[26] DNA-aptamers are considered as interesting alternatives to common ligand moieties such as peptides, small molecules, polysaccharides, and antibodies. Due to several advantages of DNA-aptamers including high stability, low or no immunogenicity, easy modification, cost-effectiveness, and lower batch-to-batch variation, they can be used for active targeting and controlled drug delivery.[27,28] We previously conjugated the EpCAM aptamer on the surface of magnetic mesoporous silica nanoparticles (SPION@MSNs) to achieve specific recognition of CRC cells and improve drug delivery performance.[29]

To implement a multimodal therapeutic strategy, in this study, we designed a targeted radiosensitive nano-delivery system aimed at concurrently enhancing the anti-cancer drug availability and ionizing irradiation sensitivity in the desired lesion area, for the first time. To reach this goal, the ZIF-8 platform acted as a nanocarrier to simultaneously encapsulate both anti-cancer drug (DOX) and a radiosensitizer agent (GQD). Thanks to the X-ray absorption capability of GQD, it has the potential to synergistically enhance the efficacy of RT, leading to more effective destruction of CRC cells. In the next step, the nano-delivery platform was modified with heterobifunctional polyethylene glycol (PEG) to improve its colloidal stability, resulting in a non-targeted formulation. Finally, to achieve targeted delivery of the NPs, we introduced the EpCAM aptamer on the outer surface of the therapeutic nano-platform. This strategic addition aimed to selectively recognize HT-29 cells and facilitate the delivery of both DOX and GQD. The prepared therapeutic nano-platform exhibited a significant radiosensitization effect at the tumor site upon irradiation, resulting in a synergistic antitumor efficacy of chemotherapy and RT. Consequently, this approach led to the destruction of HT-29 cancer cells and significant inhibition of tumor growth. As expected, the Apt-PEG-DOX/ZIF-8@GQD nano-platform showed remarkable combined chemo/radio/targeted efficacy both *in vitro* and *in vivo*.

Published on 02 Januari 2024. Downloaded on 19/07/2025 18:32:17.

# 2. Materials and methods

## 2.1. Materials

$Zn(NO_3)_2{\cdot}6H_2O$, 2-methylimidazole (2-MIM), 1-ethyl-3-(3-dimethylaminopropyl) carbodiimide hydrochloride (EDC), *N*-hydroxysuccinimide (NHS), 4′,6-diamidino-2-phenylindole (DAPI), and Giemsa dye were obtained from Sigma-Aldrich (Germany). GQDs (1 mg $ml^{-1}$) were purchased from Kara Pajuhesh Amirkabir (Iran). The heterobifunctional PEG polymer with a terminal α-amine hydrochloride-ω-carboxylic acid functional group ($HCl{\cdot}H_2N$–PEG–COOH, $M_w$: 3500 Da) was provided by JenKem (USA). Roswell Park Memorial Institute 1640 (RPMI 1640) medium, fetal bovine serum (FBS), trypsin-EDTA, phosphate-buffered saline (PBS), and other cell culture reagents were bought from Gibco (Scotland). Matrigel® matrix (DLW354263) was obtained from Corning Inc. (USA). An annexin V-FITC apoptosis detection kit with propidium iodide (PI) was supplied by BioLegend (USA). 3-(4,5-dimethylthiazol-2-yl)-2,5-diphenyl-2*H*-tetrazolium bromide (MTT) was purchased from Tinab Shimi (Iran). DOX was obtained from Azista Industries Pvt. Ltd (India). The 48 mer EpCAM DNA aptamer, also known as SLY3C,[30] (5′-amine CAC TAC AGA GGT TGC GTC TGT CCC ACG TTG TCA TGG GGG GTT GGC CTG-3′ thiol) was ordered from MicroSynth (Switzerland). Agarose powder, DNA marker (50 bp), and tris–borate-EDTA (TBE) buffer were purchased from DENAzist Asia (Iran). All the chemicals were commercially used without further purification.

Two cell lines including human colon cancer cells (HT-29) and Chinese hamster ovary (CHO) cells were provided by the Pasteur Institute, Tehran, Iran, and cultured in RPMI 1640 medium supplemented with 10% (v/v) FBS.

## 2.2. Synthesis of the DOX/ZIF-8@GQD nano-delivery system

The DOX/ZIF-8@GQD system was prepared following the method described by Tian *et al.* with minor modifications.[21] 25 mg of $Zn(NO_3)_2{\cdot}6H_2O$ was dissolved in 10 ml of deionized water and shaken for a short duration. Then, 2 ml of DOX solution (2 mg $ml^{-1}$) was added to the above mixture and stirred for about 30 min. 50 mg of 2-MIM in 10 ml of deionized water was then added dropwise into the above solution. After 15 min of stirring at room temperature, 1 ml of GQD solution (1 mg $ml^{-1}$) was added into the mixture with magnetic agitation for 1 h. Finally, the obtained DOX/ZIF-8@GQD was collected by centrifugation (6000*g*, 15 min) and washed at least three times with deionized water. The powder product was dried under vacuum at 60 °C for 5 h and stored for future characterization. Moreover, ZIF-8 was synthesized as a backbone nano-scaled formulation, similar to DOX/ZIF-8@GQD, without the addition of DOX and GQD solutions.[31]

The amount of DOX loaded in the ZIF-8@GQD nano-delivery system was determined using ultraviolet-visible spectrophotometry (UV/vis; Eppendorf, Germany) by measuring the absorbance at 480 nm according to the calibration curve of DOX. Finally, drug loading capacity (DLC%) and drug encapsulation efficiency (DEE%) were calculated using the following eqn (1) and (2):[32]

$$\mathrm{DLC\%} = \frac{\text{Total DOX used in the solution} - \text{DOX remained in the supernatant}}{\text{Weight of nanosystem taken}} \times 100 \quad (1)$$

$$\mathrm{DEE\%} = \frac{\text{Total DOX used in the solution} - \text{DOX remained in the supernatant}}{\text{Total DOX used in the solution}} \times 100 \quad (2)$$

## 2.3. Preparation of the non-targeted nano-delivery system (PEG-DOX/ZIF-8@GQD)

In order to improve the physicochemical properties of the nano-delivery system, bifunctional PEG ($HCl{\cdot}H_2N$–PEG–COOH) was used for surface coating. 20 mg of DOX/ZIF-8@GQD was dispersed in a solution containing 4 ml of deionized water and 60 mg $ml^{-1}$ $HCl{\cdot}H_2N$–PEG–COOH, which was heated to 60 °C and vigorously stirred for 3 h. Thereafter, the non-targeted nano-delivery system was collected by centrifugation (6000*g*, 15 min) and washed three times with deionized water to remove the non-grafted PEG, and finally dried at 50 °C in a vacuum for 6 h.[33,34]

## 2.4. Decoration of the nano-delivery system with a targeting ligand (Apt-PEG-DOX/ZIF-8@GQD)

The EpCAM aptamer was coupled with the nano-delivery system for specific targeting of EpCAM overexpressing HT-29 cells. Typically, 10 mg of PEG-DOX/ZIF-8@GQD from the previous step was well dispersed in 5 ml of deionized water with 6.54 mg of EDC and 3.92 mg of NHS under mild agitation. Subsequently, the EpCAM aptamer (30 μl, 50 μM) was added to the mixture and stirred at 4 °C overnight. Apt-PEG-DOX/ZIF-8@GQD was centrifuged at 4000*g* for 10 min to eliminate the EDC and NHS; and resuspended in 200 μl of PBS (pH 7.4). The electrostatic interactions between carboxylic acid groups of the PEGylated nano-delivery system and amine groups of the EpCAM aptamer are the main precursors to the targeted formulation. In the next step, to check the development of the Apt-PEG-DOX/ZIF-8@GQD nano-platform, electrophoresis was performed on a 2% agarose gel.[35]

## 2.5. Characterization of the nano-delivery system

Fourier transform infrared (FTIR) spectra were recorded with an AVATAR 370 spectrometer (Thermo Nicolet, USA) in the range of 400–4000 $cm^{-1}$. Powder X-ray diffraction (PXRD) was performed on a Philips PW1730 X-ray powder diffractometer equipped with a Cu sealed tube ($\lambda$ = 1.54056 Å) at 40 kV and 30 mA. Thermogravimetric analysis (TGA) was carried out from 40 °C to 800 °C at a heating rate of 20 °C $min^{-1}$ using a Q600 thermal analyzer (TA, USA). Energy-dispersive X-ray (EDX) mapping analysis was performed to determine the elemental composition (C, N, O and Zn) using a SEM equipped with an EDX apparatus (MIRA III, Czech Republic). The specific surface area and pore size distribution were computed by Brunauer–Emmett–Teller (BET) and Barrett–Joyner–Halenda (BJH) methods, respectively, which were performed using BELSORP MINI II, Japan. The size distribution and surface zeta potential values of nanoparticles were measured using a dynamic light scattering equipment (DLS; VASCO-3, France) and a zeta potential analyzer (Zeta Compact, France), respectively. Atomic force

 This journal is © The Royal Society of Chemistry 2024

Published on 02 Januari 2024. Downloaded on 19/07/2025 18:32:17.

microscopy (AFM; JPK NanoWizard II, Germany), field emission-scanning electron microscopy (FE-SEM; MIRA III, Czech Republic), and transmission electron microscopy (TEM; Philips CM120, Netherlands) were utilized to visualize the morphology and shape of the prepared nano-delivery system.

### 2.6. pH-triggered DOX release from the nano-delivery system

pH-sensitive dissolution is the prominent characteristic of ZIF-8 that can be used to achieve high local concentration of anti-cancer drugs.[36] The pH-responsive release of DOX from both PEG-DOX/ZIF-8@GQD and Apt-PEG-DOX/ZIF-8@GQD was evaluated at pH values of 7.4 (physiological pH) and 5.4 (acidic pH). To conduct the release experiments, the samples were individually dispersed in 1 ml of PBS solution with pH values of 7.4 and 5.4, followed by transfer into two separate dialysis membranes with a cutoff of 1000 Da. Afterwards, the dialysis bags were immersed into 3 ml of corresponding PBS solutions at 37 °C and shaken at 60 rpm for 96 h in the dark. At regular time intervals, 3 ml of the solution was taken out and the absorbance was recorded at 480 nm to measure the cumulative DOX release percentages. Simultaneously, 3 ml of fresh solution was replenished into the dialysis solution to maintain the volume constant.[37]

### 2.7. Verifying the PEGylation effects on blood compatibility

In this study, we investigated and compared the disruption of red blood cells (RBCs) after treatment with DOX/ZIF-8@GQD and PEG-DOX/ZIF-8@GQD through a hemolysis assay. To achieve this aim, healthy volunteer blood specimens were collected and centrifuged for 10 min at 1500*g* five times and re-suspended in 10 ml of PBS buffer. Then 100 μl of RBC suspension was mixed with 900 μl of various concentrations of nanoparticles (12.5 to 200 μg $ml^{-1}$) in PBS and incubated at 150 rpm for 12 and 24 h. After each time period, the mixture was centrifuged and the related absorbance of the supernatant was monitored using an enzyme linked immunosorbent assay (ELISA reader; Awareness Technology, USA) at 570 nm. It should be noted that, RBCs incubated with distilled water and PBS were regarded as positive (100% lysis) and negative (0% lysis) control groups.[38] The percentage of hemolysis was calculated *via* the following eqn (3):

$$\text{Hemolysis ratio}\% = \frac{\text{Absorbance of sample} - \text{Absorbance of negative control}}{\text{Absorbance of positive control} - \text{Absorbance of negative control}} \times 100 \quad (3)$$

### 2.8. *In vitro* cytotoxicity studies

**2.8.1. MTT assay.** The anti-cancer properties of non-targeted and targeted nano-delivery systems were compared on EpCAM positive (HT-29) and negative (CHO) cell lines using the MTT assay. HT-29 and CHO cells were seeded in 96-well plates with a density of $8 \times 10^3$ cells per well and cultured at 37 °C overnight. The following day, both cell types were treated with fresh media containing different concentrations of free DOX, PEG-DOX/ZIF-8@GQD, and Apt-PEG-DOX/ZIF-8@GQD (3.12 μg $ml^{-1}$ to 100 μg $ml^{-1}$; equivalent concentrations of DOX). After 24, 48, and 72 h of incubation, the medium of each well was replaced with fresh culture medium containing 10% MTT (5 mg $ml^{-1}$ in PBS) and incubated at 37 °C for 3 h. Afterwards, to dissolve formazan crystals, 150 μl of dimethyl sulfoxide (DMSO) was added to each well and the optical density (OD) was then determined at 570 nm using an ELISA reader.

**2.8.2. Clonogenic assay.** The colony formation assay (CFA) was performed to assess cell survival following RT *in vitro*. HT-29 and CHO cells were cultured in 96-well plates, as mentioned above, for 24 h. The cells were set in three groups including the control, radiation only (3 Gy), and targeted nano-delivery system plus ionizing radiation (IR; 3 Gy). The combination group was treated with different concentrations of Apt-PEG-DOX/ZIF-8@GQD (100, 50, and 25 μg $ml^{-1}$; equivalent concentrations of DOX) for 4 h and then exposed to radiation using an X-ray linear accelerator (Philips, dose rate: 200 Mu $min^{-1}$). Immediately after irradiation, cells were trypsinized, counted, and re-seeded into 6-well plates at a density of 2000 cells per well for another 10 days at 37 °C under a humidified atmosphere with 5% $CO_2$. Finally, the colonies were stained with Giemsa, counted and plotted as the survival fraction (SF).[11]

**2.8.3. Cellular uptake of nano-delivery systems.** The cellular uptake of nano-delivery systems was validated using both fluorescence microscopy and flow cytometry techniques. HT-29 and CHO cells were seeded in 6-well plates at a density of $2 \times 10^5$ cells per well for 24 h and divided into four groups (free DOX, PEG-DOX/ZIF-8@GQD, Apt-PEG-DOX/ZIF-8@GQD, and Apt-PEG-DOX/ZIF-8@GQD + RT; the final concentration of DOX in all the nano-delivery systems was 5 μg $ml^{-1}$). For combination treatment, both cell types were first treated with Apt-PEG-DOX/ZIF-8@GQD, and 3 Gy IR exposure was carried out after 4 h.[24] For fluorescence microscopy, as a qualitative technique, cells were washed with PBS and then fixed in 4% paraformaldehyde for 15 min. Then, the cells were stained with DAPI to localize nuclei. Finally, the uptake of nano-delivery systems was determined using a fluorescent microscope (Olympus BX51, Japan). The cellular uptake of nanoplatforms was further confirmed by flow cytometry as a quantitative method. For this purpose, after 6 h of treatment, cells were detached using trypsin-EDTA and collected by centrifugation at 400*g* for 15 min. Cells were re-suspended in 300 μl of PBS and immediately assessed with flow cytometry (BD Accuri C6, USA) in the FL2 channel to determine the fluorescence intensity.

**2.8.4. Determination of the cell death mechanism.** To evaluate the mode of cell death, $2 \times 10^5$ HT-29 cells were seeded in 6-well plates and incubated overnight. Afterwards, the media containing free DOX, PEG-DOX/ZIF-8@GQD and Apt-PEG-DOX/ZIF-8@GQD with a final DOX concentration of 2 μg $ml^{-1}$ were used to replace the culture media. In the combination treatment group, cells were treated with Apt-PEG-DOX/ZIF-8@GQD for 4 h,

Published on 02 Januari 2024. Downloaded on 19/07/2025 18:32:17.

followed by 3 Gy irradiation.[39] Radiation alone (3 Gy) was also used as the fifth experimental group for further comparison. After 24 h of incubation, HT-29 cells were stained using an annexin V-FITC kit with PI, and the results were assessed through flow cytometry and analyzed using FlowJo 7.6 software.

### 2.9. Development of a xenograft mouse model

All mice were kept in an animal house at Ferdowsi University of Mashhad (FUM) and experiments were conducted in accordance with protocols approved by the Animal Ethics Committee of FUM (IR.UM.REC.1400.032). An immunosuppression protocol was carried out on male C57BL/6 mice (4–6 weeks old) as described previously.[40] The xenograft tumor model was developed by subcutaneous injection of $8 \times 10^6$ HT-29 cells (suspended in 1 : 1; PBS: Matrigel) into the back of immunocompromised C57BL/6 mice.

**2.9.1. *In vivo* anti-tumor efficacy.** Treatments began when the tumor volume reached an average size of 70–100 $mm^3$ after cell implantation. Immunocompromised C57BL/6 mice bearing human HT-29 tumors were randomly assigned to seven different experimental groups: (1) control (PBS treatment without nano-delivery systems and radiation), (2) free DOX (1 mg $kg^{-1}$), (3) non-targeted group (PEG-DOX/ZIF-8@GQD; 1 mg $kg^{-1}$ of DOX in 100 μl nanoparticles), (4) targeted group (Apt-PEG-DOX/ZIF-8@GQD; 1 mg $kg^{-1}$ of DOX in 100 μl nanoparticles), (5) RT alone (3 Gy), (6) combination group (Apt-PEG-DOX/ZIF-8@GQD + RT), and (7) DOX + RT. The treated mice were administered either a single tail-vein injection (groups 1, 2, 3, 4, 6 and 7) or a single dose of 3 Gy radiation (group 5). Moreover, 24 h after injection of targeted nanoplatforms in group 6 and free DOX in group 7, the HT-29 tumor-bearing C57BL/6 mice were exposed to a single dose of 3 Gy radiation.[41] The body weights and tumor volumes were checked every other day for a period of 15 days. At the end of the treatment period, mice were sacrificed and some organs including the liver, spleen, lungs, kidneys, heart, and tumor, were dissected. Tissues were then stained with hematoxylin and eosin (H&E) in order to check the possible side effects.

**2.9.2. *In vivo* bio-distribution of nano-delivery systems.** To assess the safety of nano-scaled formulations, the systematic distribution of nano-delivery systems was monitored *in vivo* and compared with free DOX. It should be noted that DOX was also selected as the indicator for *in vivo* tracking purposes due to its self-fluorescence. The biological distribution of free DOX (+RT), PEG-DOX/ZIF-8@GQD, and Apt-PEG-DOX/ZIF-8@GQD (+RT) with an equivalent amount of 1 mg $kg^{-1}$ DOX was assessed after 12, 24, and 48 h of intravenous injection into C57BL/6 mice bearing human HT-29 tumors. In the combinatorial treatment groups, Apt-PEG-DOX/ZIF-8@GQD and DOX were injected intravenously and after 4 h, the tumors were exposed to 3 Gy radiation. The organs (liver, spleen, lungs, kidneys, heart, and tumor) were carefully removed and their fluorescence intensities were evaluated using an *in vivo* imaging system (IVIS; KODAK, USA).

### 2.10. Statistical analysis

All statistical comparisons were undertaken using GraphPad Prism software 9.3.0 (San Diego, CA). Statistical significance was evaluated by one-way analysis of variance (ANOVA) or Student's *t*-test with Tukey's multiple comparisons. Experiments were performed at least three times in triplicate. $*p < 0.05$ was determined to be statistically significant.

## 3. Results and discussion

### 3.1. Characterization of the synthesized nano-delivery systems

DOX/ZIF-8@GQD was first synthesized by a one-pot method and characterized by FTIR spectroscopy, and then the FTIR spectrum of DOX/ZIF-8@GQD was compared with that of ZIF-8, serving as a backbone. Fig. S1 (ESI†) shows that the band corresponding to Zn–N stretching is located at 421 $cm^{-1}$. The C–N stretching bands appeared at 1145 and 995 $cm^{-1}$, indicating the presence of imidazole units, and a peak at 1576 $cm^{-1}$ was attributed to the C═N stretching vibration of DOX/ZIF-8@GQD. The FTIR peaks at 2924 and 3421 $cm^{-1}$ observed in DOX/ZIF-8@GQD were assigned to the O–H and C═C–H stretching of GQD, which confirms the existence of GQDs.[42,43] The PXRD patterns of ZIF-8 and DOX/ZIF-8@GQD are presented in Fig. 1A. ZIF-8 indicated narrow and strong diffraction peaks with good crystallinity and DOX/ZIF-8@GQD showed similar patterns compared to the backbone. It should be noted that no visible peaks from GQD were detected in the DOX/ZIF-8@GQD nano-delivery system, which might be attributed to the strong interaction of carboxyl, hydroxyl, and epoxy groups on GQD with N–H functional groups of 2-MIM during the one-pot synthesis procedure, leading to the successful introduction of GQD into the ZIF-8 nano-delivery system. Our findings are entirely consistent with previous reports on ZIF-8@GQD which demonstrated that ZIF-8 could provide specific interaction sites for GQD.[21,44,45] The TGA curves of ZIF-8 and DOX/ZIF-8@GQD are also shown in Fig. 1B. For ZIF-8, the weight loss occurred in one step at 500 °C corresponding to the removal of inorganic units. Moreover, the weight loss in the range of 200–250 °C for DOX/ZIF-8@GQD is attributed to the degradation of GQD, which is confined within the ZIF-8. The EDX mapping of DOX/ZIF-8@GQD confirmed the presence of main elements in the nano-delivery system (Fig. S2, ESI†). Based on the above results, the introduction of GQD into the ZIF-8 nano-delivery system was successfully established. To check the inclusion of DOX inside ZIF-8 during the synthesis procedure, $N_2$ adsorption isotherms, porosity, DLC%, and DEE% were measured. Sufficient porosity in nano-scaled carriers is a crucial parameter for achieving excellent effects of RT and chemotherapy in combination treatment. As illustrated in Fig. 1C, the $N_2$ adsorption/desorption isotherms for both ZIF-8 and DOX/ZIF-8@GQD exhibited a typical type I curve, which is considered to be the main feature of microporous materials.[46] The BET surface area of ZIF-8 was 1013 $m^2$ $g^{-1}$, while the surface area of DOX/ZIF-8@GQD was considerably reduced to 110 $m^2$ $g^{-1}$. In addition, the corresponding pore volumes of ZIF-8 and DOX/ZIF-8@GQD were 0.47 and 0.14 $cm^3$ $g^{-1}$, respectively. Our results are consistent with other reports indicating that a clear reduction of the BET surface area and BJH pore volume is related to an increased

 This journal is © The Royal Society of Chemistry 2024

Published on 02 Januari 2024. Downloaded on 19/07/2025 18:32:17.

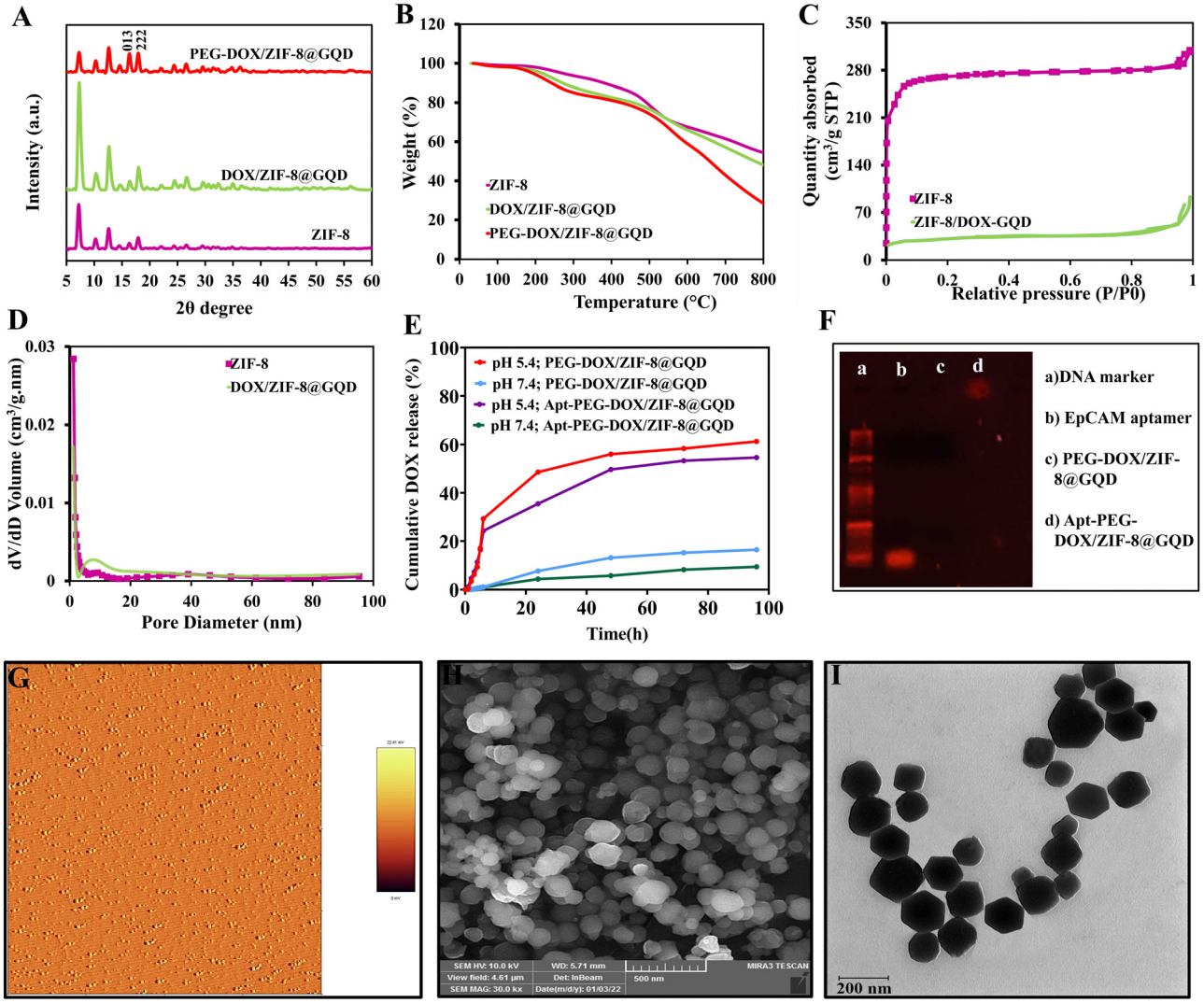


Fig. 1 Physicochemical characterization of the synthesized nano-delivery systems. (A) PXRD patterns and (B) TG analysis of ZIF-8, DOX/ZIF-8@GQD and PEG-DOX/ZIF-8@GQD. (C) $N_2$ adsorption/desorption isotherms and (D) pore size distribution of ZIF-8 and DOX/ZIF-8@GQD. (E) Drug release profile of PEG-DOX/ZIF-8@GQD and Apt-PEG-DOX/ZIF-8@GQD under two different conditions with pH 7.4 and pH 5.4 (data are presented as mean ± SD, $n$ = 3). (F) The conjugation of the EpCAM aptamer to PEG-DOX/ZIF-8@GQD was confirmed by gel electrophoresis. The morphology of Apt-PEG-DOX/ZIF-8@GQD samples was characterized using (G) AFM, (H) FE-SEM and (I) TEM analyses. Abbreviations: PXRD; powder X-ray diffraction, TGA; thermogravimetric analysis, ZIF-8; zeolitic imidazolate framework-8, DOX; doxorubicin, GQD; graphene quantum dot, PEG; polyethylene glycol, Apt; aptamer, EpCAM; epithelial cell adhesion molecule, FE-SEM; field emission-scanning electron microscopy and TEM; transmission electron microscopy.

proportion of DOX inside the ZIF-8. For instance, Feng *et al.* showed that the specific surface area of ZIF-8 was markedly shifted from 1885.258 to 1544.752 $m^2\ g^{-1}$ after simultaneous encapsulation of DOX and MXene quantum dots (MQDs).[47] Moreover, the pore size distributions of ZIF-8 (1.88 nm) and DOX/ZIF-8@GQD (5.07 nm) mainly appeared as micropores and mesopores, respectively (Fig. 1D). It can be deduced that the confined DOX within the micropores and the presence of $N_2$ gas in the mesopores[48] resulted in the larger pore size of DOX/ZIF-8@GQD compared to ZIF-8. Another evidence of the successful embedment of DOX inside ZIF-8 can be confirmed by the DLC% and DEE%, which were approximately 37.5% and 90%, respectively. Moreover, the results of zeta potential and particle size of DOX/ZIF-8@GQD were consistent with GQD and DOX encapsulation data (Table 1). The results of zeta potential analysis showed that ZIF-8 has a positive charge (+7.215 ± 2.01 mV) and the simultaneous encapsulation of GQD and DOX during the one-pot synthesis procedure caused a negative shift in the zeta potential of the DOX/ZIF-8@GQD sample (−20.23 ± 1.02 mV), which is attributed to the negative charge of GQD. Additionally, the DLS assay indicated that the average particle size of DOX/ZIF-8@GQD changed to 39.92 ± 2.27 nm, which is larger than that of ZIF-8 (25.51 ± 1.90). The specific interaction between precursors of ZIF-8 and functional groups of cargos (DOX/GQD) lead to an increase in the size of nano-delivery system. Kaur *et al.* used a one-pot synthesis method to introduce anti-cancer drug 6-mercaptopurine (6-MP) into the ZIF-8 and they also reported an increasing particle size upon trapping the cargo (80 to 200 nm; from SEM analysis).[49]

Published on 02 Januari 2024. Downloaded on 19/07/2025 18:32:17.

In order to enhance biocompatibility and blood circulation of nano-delivery systems, heterobifunctional PEG was distributed on the surface of DOX/ZIF-8@GQD and a non-targeted formulation, PEG-DOX/ZIF-8@GQD, was prepared in the next step of the experiment. It has been shown that PEG concentration and reaction temperature play crucial roles in tuning the size of nanoparticles and Yu *et al.* synthesized various PEG@ZIF-8 nanoparticles in the range of 60 to 590 nm by changing both mentioned factors.[34] Similarly, Wu *et al.* obtained the PEG-decorated ZIF-8 nanoparticles *via* introducing amino-PEG to the reaction mixture (temperature at 60 °C for 3 h) based on a post-synthetic modification strategy.[33] With regard to these reports, HCl·$H_2$N–PEG–COOH covered the surface of DOX/ZIF-8@GQD through covalent bonds. Following PEGylation, the absorption bands at 2871 and 2927 $cm^{-1}$ were assigned to the $CH_2$ groups in the PEG polymer (Fig. S1, ESI†).[50] The PXRD pattern of PEG-DOX/ZIF-8@GQD aligns well with that of the DOX/ZIF-8@GQD (Fig. 1A). The PEG-DOX/ZIF-8@GQD exhibited two major peaks corresponding to (011) and (013) planes, which could be due to the interactions between amino group of PEG and negative groups of backbone during the modification process.[34] In order to obtain conclusive evidence of the coverage of bifunctional PEG on the surface of DOX/ZIF-8@GQD, TGA was performed. The typical temperature for PEG degradation is located in the range of 350–500 °C,[51] matching well with our TGA results (Fig. 1B). EDX analysis of PEG-DOX/ZIF-8@GQD clearly demonstrated the presence of the expected elements (C, N, O, and Zn) in the composition (Fig. S2, ESI†). Moreover, an increase in the average particle size (76.83 ± 4.00 nm) and a slight decrease in zeta potential (−13.66 ± 1.43 mV) of PEG-DOX/ZIF-8@GQD can be ascribed to the incorporation of PEG on the surface of DOX/ZIF-8@GQD. Similarly, Guo *et al.* reported that the particle size of dextran-modified Cy5.5&ICG@ZIF-8 nanocomposites (170 nm) was larger than those which were not decorated with dextran (135 nm).[52] As mentioned earlier, ZIF-8 turned out to be a favorable vehicle for controlled drug delivery due to its stability under normal physiological conditions. Based on this property, the behavior of DOX release from both non-targeted and targeted platforms was evaluated at pH 7.4 and 5.4. At neutral pH, only 7.6% of DOX was released after 24 h, and a maximum of 16.4% was released after 96 h from PEG-DOX/ZIF-8@GQD. Similarly, for Apt-PEG-DOX/ZIF-8@GQD, only 4.26% of DOX was released after 24 h, and a maximum of 9.36% was released after 96 h. Interestingly, a distinct behavior was observed for both nanoplatforms at pH 5.4 in comparison to pH 7.4. The coordination bonds between zinc ions and 2-MIM rings are dissociated in an acidic environment, which results in the decomposition of ZIF-8.[53,54] The cumulative release of DOX from both non-targeted and targeted platforms was found to reach up to 61.26% and 54.61%, respectively, within 96 h. Fig. 1E illustrates two consecutive stages of release, characterized by a rapid initial release followed by a gradual release, for both nanoplatforms at pH 5.4. These findings indicate that the release of DOX from PEG-DOX/ZIF-8@GQD and Apt-PEG-DOX/ZIF-8@GQD vehicles exhibits on-demand features and prolonged release performance. This property is advantageous for enhancing the cytotoxicity of DOX towards cancerous cells. Extracellular matrix (ECM), the presence of various cells (cancer stem cells, cancer cells, normal cells, supporting cells *etc.*), and defective vascular networks are three fundamental components of the TME.[55] In this context, nanoparticles with a size ranging from 10 to 100 nm can easily cross through leaky tumor vasculature and accumulate at the lesion tissue *via* enhanced permeability and retention (EPR) effect, which is known as passive targeting.[56] In the next step, employing an active targeting strategy enables the specific recognition of cancerous cells and successful delivery of therapeutic drugs. Utilizing this concept, we designed the surface of PEG-DOX/ZIF-8@GQD with the EpCAM aptamer to develop a targeted nano-delivery system. The electrostatic interactions between active carboxylic acid groups of heterobifunctional PEG and amine groups of the EpCAM aptamer resulted in the formation of amide bonds in Apt-PEG-DOX/ZIF-8@GQD, which was further confirmed by agarose gel electrophoresis. As displayed in Fig. 1F, the free EpCAM aptamers migrated to the location of 50 bp. However, PEG-DOX/ZIF-8@GQD did not show any band, while Apt-PEG-DOX/ZIF-8@GQD NPs were visible in the loaded well due to their larger size, suggesting the successful preparation of the targeted nano-delivery system. In order to observe the morphology of the final nano-scaled delivery system, AFM, TEM, and FE-SEM analyses were performed and the results exhibited some rhomboid shaped particles with a uniform dispersion of Apt-PEG-DOX/ZIF-8@GQD exhibiting an average particle size of ~100 nm (Fig. 1G–I); these findings are in agreement with previous studies.[21,43] Moreover, a similar trend in diameter was demonstrated in the TEM images and DLS results of Apt-PEG-DOX/ZIF-8@GQD.

### 3.2. Development of a hemocompatible nano-delivery system

Medical applications of nano-delivery systems lead to their direct interaction with healthy tissues and blood. In this regard, nano-platforms should be designed properly to prevent several

Table 1 The average values of zeta potential, particle size and polydispersity index (PDI) of all different formulations synthesized in this study

| Sample | Zeta potential (mV) | Particle size (nm) | Polydispersity index (PDI) |
|---|---|---|---|
| ZIF-8 | +7.215 ± 2.01 | 25.51 ± 1.90 | 0.21 ± 0.01 |
| DOX/ZIF-8@GQD | −20.23 ± 1.02 | 39.92 ± 2.27 | 0.23 ± 0.01 |
| PEG-DOX/ZIF-8@GQD | −13.66 ± 1.43 | 76.83 ± 4.00 | 0.19 ± 0.02 |
| Apt-PEG-DOX/ZIF-8@GQD | −9.60 ± 1.10 | 101.19 ± 9.60 | 0.21 ± 0.01 |

Abbreviations: ZIF-8; zeolitic imidazolate framework-8, DOX; doxorubicin, GQD; graphene quantum dot, PEG; polyethylene glycol and EpCAM; epithelial cell adhesion molecule.

 This journal is © The Royal Society of Chemistry 2024

Published on 02 Januari 2024. Downloaded on 19/07/2025 18:32:17.

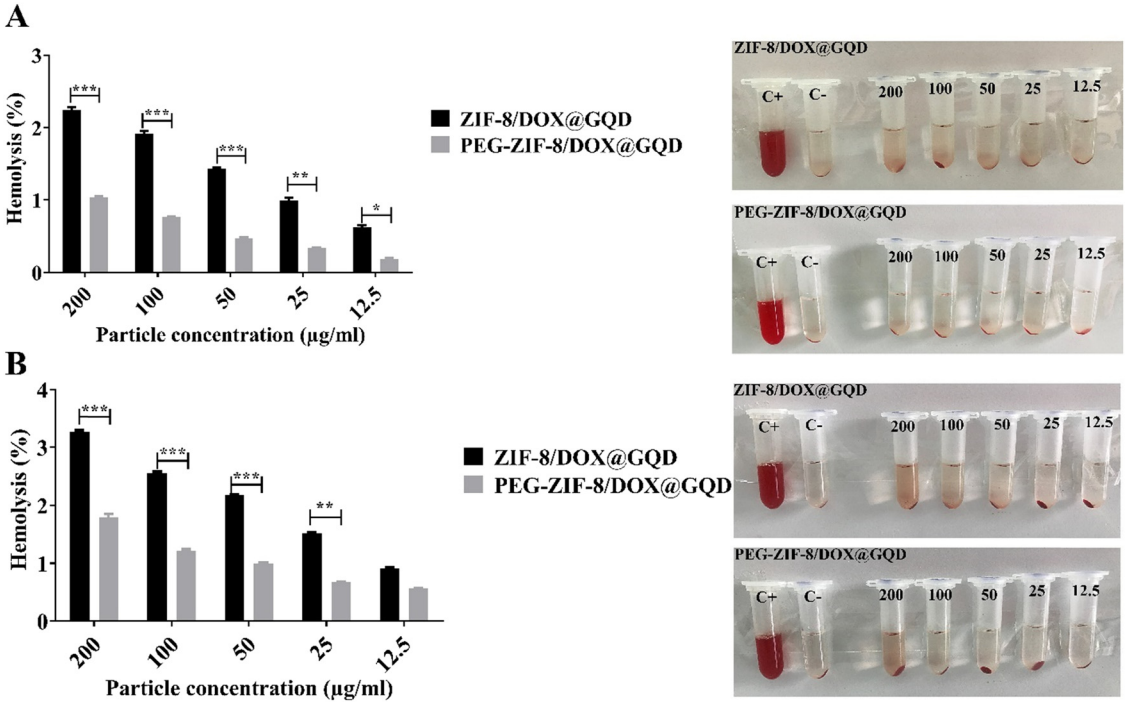


Fig. 2 Hemocompatibility comparison of the nano-delivery systems before and after being coated with PEG. Hemolysis percentage induced by nano-delivery systems and visual inspection of tubes after (A) 12 h and (B) 24 h. The values presented in the graphs are mean ± SD of triplicate experiments. * $p < 0.05$, ** $p < 0.01$ and *** $p < 0.001$ were considered statistically significant. Abbreviations ZIF-8; zeolitic imidazolate framework-8, DOX; doxorubicin, GQD; graphene quantum dot, PEG; polyethylene glycol, Apt; aptamer and SD; standard deviation.

problems, including hemolysis. Covering nano-vehicles with PEG, a well-known biocompatible polymer, has been proposed as a worthwhile strategy for reducing their toxicity potential and improving the biological properties.[57] In this study, the efficacy of PEGylation was investigated using a hemolysis assay, comparing it to the backbone without PEG, to assess the extent of RBC destruction. As shown in Fig. 2A, hemolytic activity of the PEG-DOX/ZIF-8@GQD formulation remained below the threshold of 2%, even at high concentrations. In contrast, the hemolysis ratio induced by 200 and 100 μg $ml^{-1}$ DOX/ZIF-8@GQD increased with time. At 200 μg $ml^{-1}$ DOX/ZIF-8@GQD, the hemolytic activity level was 2.25% at 12 h and reached 3.2% after 24 h. Lin *et al.* reported that ZIF-8 at 0.1 mg $ml^{-1}$ could be considered as a biosafe nanomaterial while at 1 mg $ml^{-1}$ or higher, it led to the destruction of RBC membranes and induced hemolysis.[58] According to the results, DOX/ZIF-8@GQD and PEG-DOX/ZIF-8@GQD showed low hemolytic (2%–5% hemolysis) and non-hemolytic (0%–2% hemolysis) behaviors, respectively.[59]

### 3.3. Selective toxicity effects *via* the aptamer-equipped nano-platform

To further evaluate the therapeutic effects and feasibility of the prepared targeted nano-platform for CRC therapy, the cytotoxicity of free DOX, PEG-DOX/ZIF-8@GQD, and Apt-PEG-DOX/ZIF-8@GQD on EpCAM positive HT-29 and EpCAM negative CHO cells was compared. Table 2 shows the corresponding $IC_{50}$ values for HT-29 and CHO cells treated with free DOX, non-targeted, and targeted formulations. The results demonstrated that due to the small size and non-specific nature of free DOX, it is toxic to both HT-29 and CHO cells owing to its rapid diffusion into the cells. Interestingly, Apt-PEG-DOX/ZIF-8@GQD exhibited a notable cell growth inhibition potency in HT-29 cells compared to PEG-DOX/ZIF-8@GQD at the same concentrations. The specific combination of the EpCAM aptamer with the overexpressed EpCAM receptors on the surface of HT-29 cells resulted in superior accumulation of the targeted nano-delivery system. Additionally, the Apt-PEG-DOX/ZIF-8@GQD nano-platform demonstrated very low toxicity on normal cells due to the low density of EpCAM receptors on the surface of CHO cells. Specific and selective anti-cancer performance is the prominent characteristic of targeted nano-delivery systems as compared to free drug and non-targeted formulations, which leads to nonobvious cytotoxicity on normal cells. Additionally, the effectiveness of Apt-PEG-DOX/ZIF-8@GQD increased significantly with increasing DOX concentration against HT-29 cells and its effect was augmented with incubation time. As evident in Fig. 3, over 90% of HT-29 cells treated with free DOX, PEG-DOX/ZIF-8@GQD, and Apt-PEG-DOX/ZIF-8@GQD at the highest concentration were killed after 72 h of incubation. Moreover, 5% and 24% of CHO cells remained viable after treatment with the same concentration of free DOX and PEG-DOX/ZIF-8@GQD, respectively. Remarkably, the viability of CHO cells was about 60% even in the presence of 100 μg $ml^{-1}$ of the targeted nano-platform. Our results are consistent with other reports, confirming that employing targeting moieties could specifically deliver chemotherapeutic agents to cancer cells and significantly decrease the adverse side effects of the anti-cancer

Table 2 $IC_{50}$ values of different treatment groups on HT-29 and CHO cells during 24, 48, and 72 h

| Treatments | $IC_{50}$ (μg ml$^{-1}$) ± SD (HT-29 cells) | | | $IC_{50}$ (μg ml$^{-1}$) ± SD (CHO cells) | | |
|---|---|---|---|---|---|---|
| | 24 h | 48 h | 72 h | 24 h | 48 h | 72 h |
| Free DOX | 17.70 ± 2.09 | 13.56 ± 1.76 | 8.50 ± 1.79 | 20.58 ± 1.79 | 16.71 ± 1.87 | 11.82 ± 1.76 |
| PEG-DOX/ZIF-8@GQD | 31.39 ± 1.91 | 20.84 ± 1.86 | 13.84 ± 1.80 | 80.02 ± 2.69 | 52.09 ± 2.14 | 38.56 ± 1.81 |
| Apt-PEG-DOX/ZIF-8@GQD | 24.26 ± 1.89 | 16.80 ± 1.79 | 11.12 ± 1.79 | 204.2 ± 1.97 | 188.6 ± 1.95 | 164.5 ± 2.07 |

Abbreviations: DOX; doxorubicin, PEG; polyethylene glycol, ZIF-8; zeolitic imidazolate framework-8, GQD; graphene quantum dot, Apt; aptamer and SD; standard deviation.

Published on 02 Januari 2024. Downloaded on 19/07/2025 18:32:17.

drugs. For instance, it has been shown that combining the AS1411 aptamer as a targeting recognition unit with porphyrinic MOF@DOX (pro-MOF) could significantly inhibit the viability of HeLa cells with no notable effect on NIH/3T3 cells.[60] Bi *et al.* conjugated folic acid (FA), as a targeting moiety, with ZIF-8 (DOX@ZIF-8-FA) for the specific recognition of human hepatocellular carcinoma HepG2 cells. Their results showed that DOX@ZIF-8-FA nanoparticles induced more effective cancer cell growth inhibition as compared to DOX@ZIF-8.[32] Sun *et al.* coated the α-TOS@ZIF-8 compound (tocopherol succinate (α-TOS) in ZIF-8) with hyaluronic acid (HA), demonstrating considerable targeting capacity to CD44 overexpressing HeLa cells. Moreover, the targeted compound, HA/α-TOS@ZIF-8, possessed negligible toxicity towards L929 normal cells.[61]

### 3.4. Targeted nano-platform improved the efficacy of RT

GQDs have indicated suitable radiation-amplifying properties, leading to the potential use of these radiosensitizers for multimodal CRC therapy.[11] In this context, a CFA was performed to determine the impact of Apt-PEG-DOX/ZIF-8@GQD on the survival and colony forming ability of HT-29 and CHO cells after exposure to IR (Fig. 4A). As shown in Fig. 4B, the targeted nano-delivery system significantly influenced the proliferation ability of the irradiated HT-29 cells. Compared with RT alone, there was a prominent decrease in HT-29 colonies when RT was applied along with Apt-PEG-DOX/ZIF-8@GQD treatment. For instance, in the case of 3 Gy RT alone and at the highest concentration of Apt-PEG-DOX/ZIF-8@GQD plus 3 Gy radiation, the number of colonies was significantly decreased to 23% and 2%, respectively, in comparison with the untreated control group (96%). This indicates the increase in radiosensitization and superior effects of multimodal therapy. In contrast, the number of colonies formed by CHO cells in the triple combination treatment groups (targeted nano-delivery systems plus 3 Gy radiation) was similar to that in the RT alone group (Fig. 4C). These results are consistent with MTT data, demonstrating that Apt-PEG-DOX/ZIF-8@GQD was capable of increasing radiosensitivity, particularly in EpCAM over-expressing HT-29 cells.

### 3.5. Enhanced cellular internalization in concurrent targeted chemotherapy and RT

The ability to recognize cancer cells and targeted delivery of therapeutic cargos are two important factors in determining the drug delivery performance. Cellular internalization of different treatment groups was monitored with both fluorescent microscopy and flow cytometry. As shown in Fig. 5A and C, DAPI staining was used to give blue color to the nuclei as compared with red fluorescence from DOX molecules that was used to show the presence of nano-formulations. In free DOX and PEG-DOX/ZIF-8@GQD groups, bright red fluorescence was detected in many cells after treatment of both HT-29 and CHO cells, indicating their nonspecific cell internalization. Moreover, strong red fluorescence was observed in both mono (targeted nano-platform) and combination (targeted nano-platform + RT) treatment groups in HT-29 cells. The red fluorescence of DOX was relatively weaker in CHO cells for Apt-PEG-DOX/ZIF-8@GQD + RT in comparison with Apt-PEG-DOX/ZIF-8@GQD alone, indicating that RT could enhance the internalization of targeted formulation in CRC cells (Fig. 5A and C). These results were also confirmed by flow cytometry, which demonstrated that the cellular uptake of Apt-PEG-DOX/ZIF-8@GQD at 3 Gy radiation was noticeably higher in HT-29 cells and lower in CHO cells compared to other experimental groups. It has been shown that RT can affect the cellular internalization of nano-platforms when combined with DDSs.[62–65] Moreover, the expression of some molecules was also altered in response to RT. The transmembrane protein Claudin7 (CLDN7) was found to be upregulated in radiation-treated gastric cancer tissues. Lee *et al.* designed liposomes equipped with the peptide targeting CLDN7 (P1-LP-DOX) and revealed an increasing uptake of DOX in gastric cancer tumors under 2 Gy radiation.[66] Yi *et al.* showed that the cellular uptake and accumulation of CuS@Melanin-PEG/DOX (CuS nanoparticles as radiosensitizers) was notably increased after 6 Gy of X-ray radiation in 4T1 cells. Changes in the cell cycle and upregulation of CLDN7 protein post IR were reported to be the main mechanisms behind these observations.[67] Furthermore, recent studies have demonstrated that local tumor radiation induces changes in the endothelial architecture of the TME, increasing its permeability, which leads to effective accumulation, distribution, and uptake of nano-delivery systems when combined with RT.[68,69] The obtained data clearly indicated that the cellular uptake of Apt-PEG-DOX/ZIF-8@GQD was maximized following RT.

### 3.6. Radiosensitivity increased the apoptotic cell death

One of the mechanisms employed to exert anti-tumor effects is induction of cancer cell death *via* apoptosis. In this study, the cell death induced in HT-29 cells was assessed by flow cytometry to compare the efficacies of mono and combination therapeutic strategies. We observed that apoptosis was the main mechanism of HT-29 cell death in all treatment groups. As shown in Fig. 5E, the percentage of apoptotic cells (early and late stages; Q2 + Q3) increased from 3.27% in the control group to 55%, 25.69%, 41.44%, 42.88%, and 83.87% in free DOX,

 This journal is © The Royal Society of Chemistry 2024

Published on 02 Januari 2024. Downloaded on 19/07/2025 18:32:17.

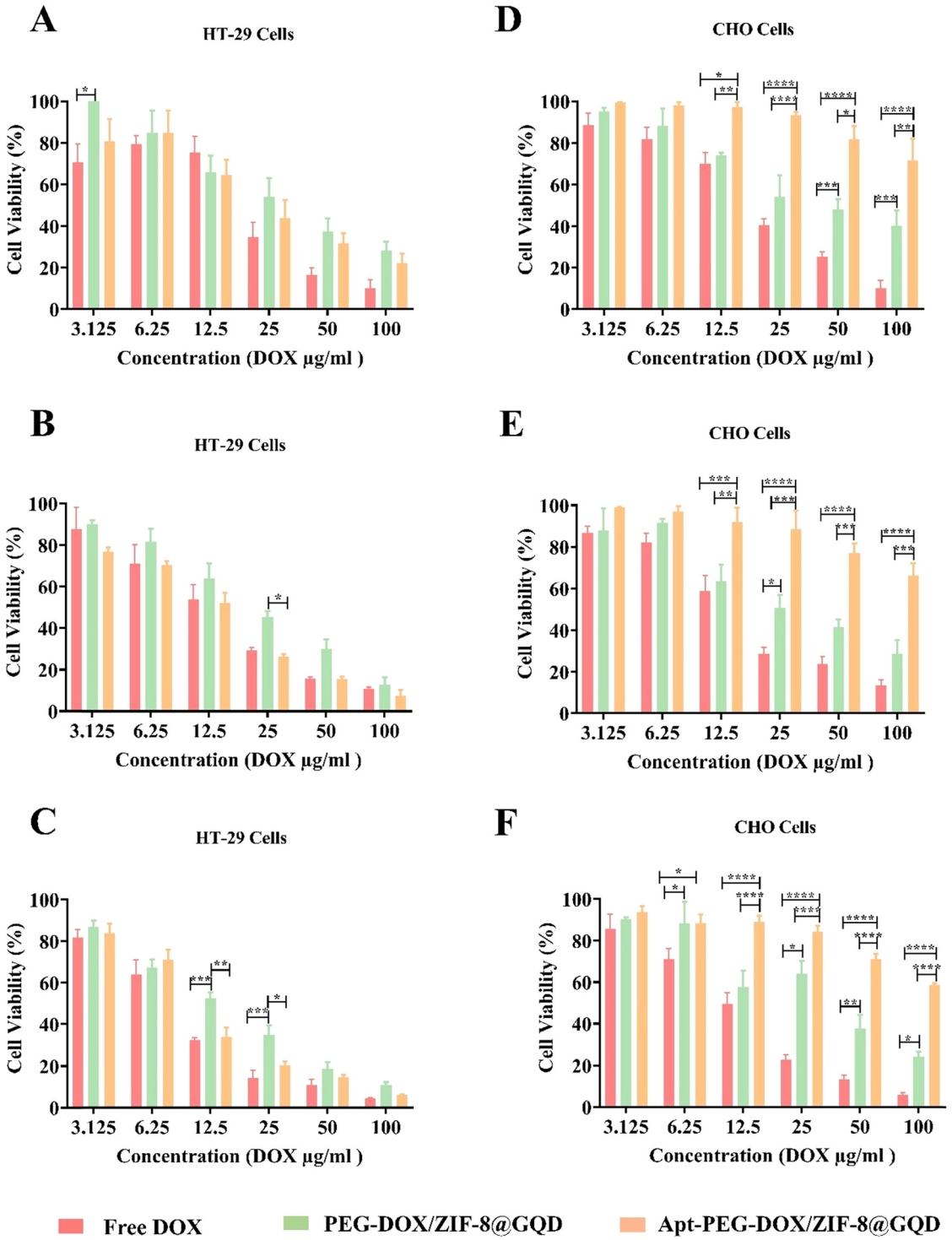


Fig. 3 Comparing the selective toxicity of different formulations on HT-29 and CHO cells. *In vitro* cytotoxicity of free DOX, PEG-DOX/ZIF-8@GQD and Apt-PEG-DOX/ZIF-8@GQD at different concentrations (3.12 μg $ml^{-1}$ to 100 μg $ml^{-1}$; equivalent concentrations of DOX) on EpCAM positive HT-29 cells after (A) 24, (B) 48 and (C) 72 h or on EpCAM negative CHO cells after (D) 24, (E) 48 and (F) 72 h of incubation. The values are shown as mean ± SD; $n = 3$, * $p < 0.05$, ** $p < 0.01$, *** $p < 0.001$ and **** $p < 0.0001$. Abbreviations: DOX; doxorubicin, PEG; polyethylene glycol, ZIF-8; zeolitic imidazolate framework-8, GQD; graphene quantum dot, Apt; aptamer and SD; standard deviation.

PEG-DOX/ZIF-8@GQD, Apt-PEG-DOX/ZIF-8@GQD, RT alone, and Apt-PEG-DOX/ZIF-8@GQD + RT groups, respectively. It is not surprising that PEG-DOX/ZIF-8@GQD did not remarkably enhance the proportion of apoptosis in comparison with the other treatment groups; however, the combination of Apt-PEG-DOX/ZIF-8@GQD with RT led to the highest level of stress and a

Published on 02 Januari 2024. Downloaded on 19/07/2025 18:32:17.

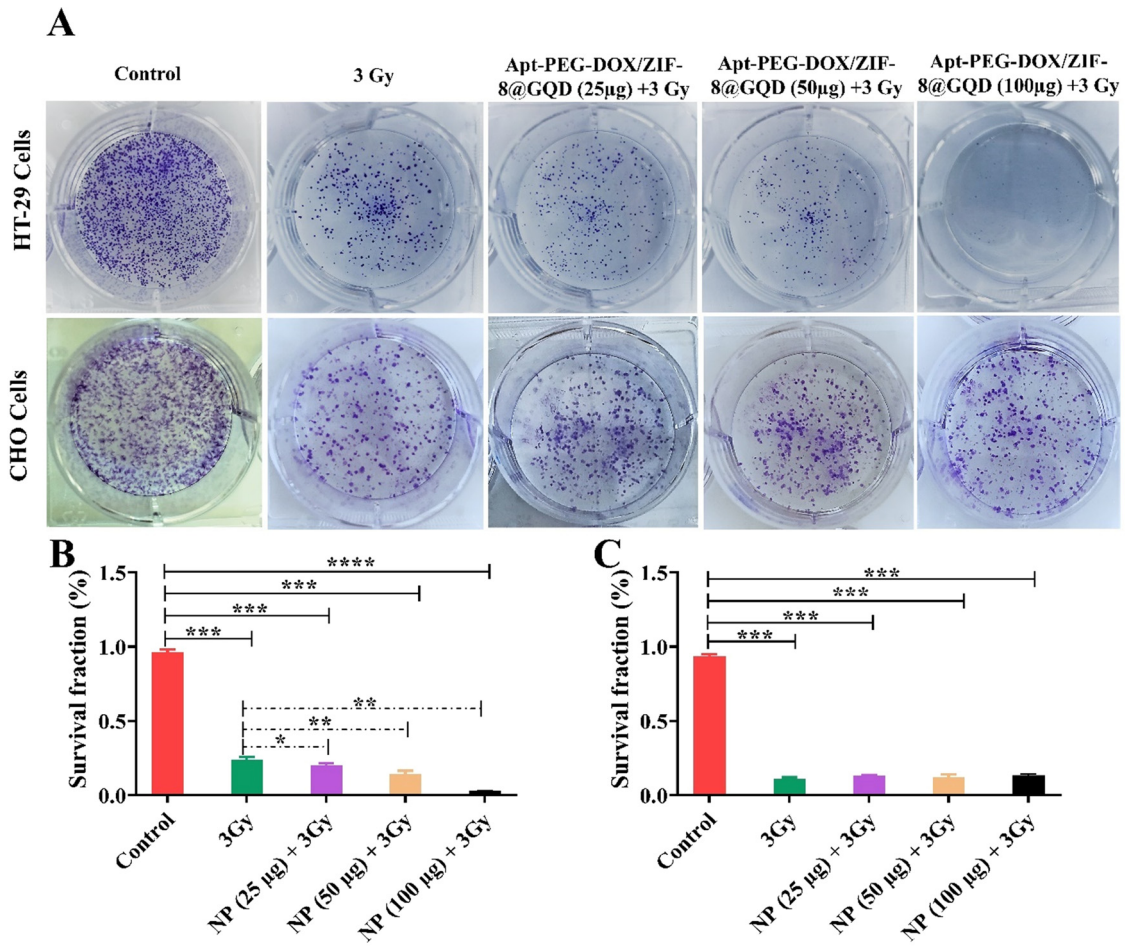


Fig. 4 Evaluating radiotherapy efficacy against HT-29 and CHO cells when combined with targeted chemotherapy. Colony formation images stained with Giemsa related to (A) EpCAM-positive HT-29 cells and EpCAM-negative CHO cells treated with Apt-PEG-DOX/ZIF-8@GQD (25, 50 and 100 μg $ml^{-1}$) and 3 Gy irradiation after 10 days. Cell survival fractions of (B) HT-29 and (C) CHO cells are presented in the diagrams. Data are presented as mean ± SD; $n = 3$; * $p < 0.05$, ** $p < 0.01$, *** $p < 0.001$ and **** $p < 0.0001$. Abbreviations: Gy; gray, Apt; aptamer, PEG; polyethylene glycol, DOX; doxorubicin, ZIF-8; zeolitic imidazolate framework-8, GQD; graphene quantum dot, and SD; standard deviation.

tendency towards apoptotic cell death. Similarly, Ni *et al.* showed that cotreatment with a nano-scale metalorganic layer (nMOL), Hf-MOL, and RT (2 Gy) significantly induced apoptosis in 4T1 breast cancer cells as compared with those treated with Hf-MOL or RT alone.[70] Zhou *et al.* reported that the combination of UiO-66-$NH_2$(Hf) and 6 Gy X-ray irradiation led to a significant increase in apoptosis in KYSE-150 cells, which was consistent with the expression of the pro-apoptotic BAX protein.[24]

### 3.7. Effective tumor growth inhibition with lower side effects achieved through a multimodal therapeutic strategy

The *in vivo* efficacy of mono and combination therapeutic approaches was systematically assessed by a series of experiments in immunocompromised mice bearing human HT-29 tumors, including tumor growth calculation, mice body-weight assessment, H&E staining, and biodistribution studies. Tumor growth curves of HT-29 tumor-bearing mice receiving different treatments are shown in Fig. 6A. As demonstrated, a rapid tumor growth was observed in the PEG-DOX/ZIF-8@GQD treatment group, indicating the less effective tumor suppression. Importantly, the difference in tumor growth was not significant between PEG-DOX/ZIF-8@GQD and PBS groups. The free DOX, Apt-PEG-DOX/ZIF-8@GQD, and DOX + RT groups presented a similar trend in suppressing tumor growth and showed a significant difference as compared with the control group ($p < 0.0001$). Moreover, RT alone did not induce great tumor growth delay in comparison with free DOX and Apt-PEG-DOX/ZIF-8@GQD groups. Not surprisingly, the combination of Apt-PEG-DOX/ZIF-8@GQD with RT indicated a significant decrease in HT-29 tumor volume, with nearly no tumor growth, as compared with other groups. This observation can be attributed to the tumor-specific internalization mediated by the EpCAM aptamer and the enhancement of radiosensitization by GQDs. By incorporating active targeting into the nanoplatform, it facilitates the selective recognition of HT-29 cancerous cells, allowing for the delivery of both chemotherapeutic and radiosensitive agents. Upon X-ray irradiation, GQDs have the ability to significantly increase the lethal efficacy of radiation, thereby resulting in superior tumor eradication outcomes. Moreover, the analysis of tumor size after 15 days of treatment showed that the HT-29

 This journal is © The Royal Society of Chemistry 2024

Published on 02 Januari 2024. Downloaded on 19/07/2025 18:32:17.

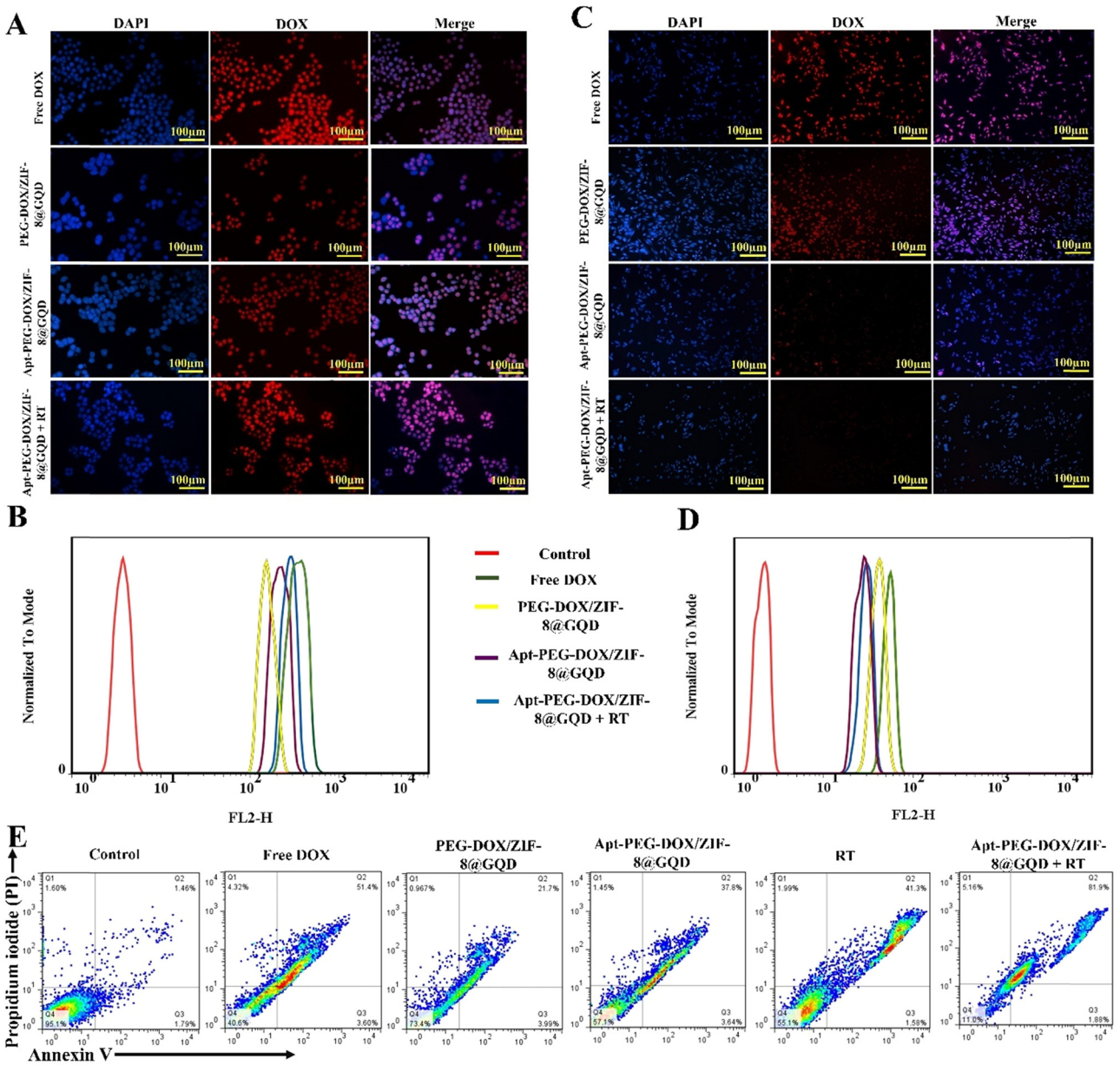


Fig. 5 Evaluation of cellular uptake and cell death mechanism in combination therapy. Fluorescence microscopy images and graphical representation of fluorescence intensity related to uptake of free DOX, PEG-DOX/ZIF-8@GQD, Apt-PEG-DOX/ZIF-8@GQD, and Apt-PEG-DOX/ZIF-8@GQD + 3 Gy radiation in (A) and (B) HT-29 and (C) and (D) CHO cells. Nuclei and nano-delivery systems were detected through blue and red fluorescence, respectively. (E) Analyzing the apoptosis induced by mono and combination therapies in HT-29 cells. Q4, Q3, and Q2 show the healthy, early and late apoptotic cell populations, respectively. Abbreviations: DAPI; 4′,6-diamidino-2-phenylindole, DOX; doxorubicin, PEG; polyethylene glycol, ZIF-8; zeolitic imidazolate framework-8, GQD; graphene quantum dot, Apt; aptamer and Gy; gray.

tumors in the combination treatment group were obviously the smallest among all groups (Fig. 6C). The anti-tumor activity of different therapeutic approaches was further confirmed by H&E staining of tumor tissues. Significant levels of cell destruction and notable levels of tumor necrosis were detected in the multimodal therapeutic group receiving Apt-PEG-DOX/ZIF-8@GQD and 3 Gy radiation concurrently (Fig. 6C). These results provide another evidence that the combination of the targeted formulation with RT led to promising anti-cancer effects *in vivo*. The clinical application of nanoplatforms has been restricted due to significant concerns regarding their toxicity.[71] In order to address this issue, three major parameters, including body weight changes, pathological toxicity, and systematic distribution of treatment agents, were analyzed to assess the toxicity and biosafety of candidate formulations in immunocompromised C57BL/6 mice. Throughout the treatments, no significant weight loss was observed in all experimental groups (Fig. 6B). Furthermore, H&E staining of the main organs (liver, spleen, lung, kidney and heart) from each treated group was conducted to estimate the possible side effects and the therapeutic application

Published on 02 Januari 2024. Downloaded on 19/07/2025 18:32:17.

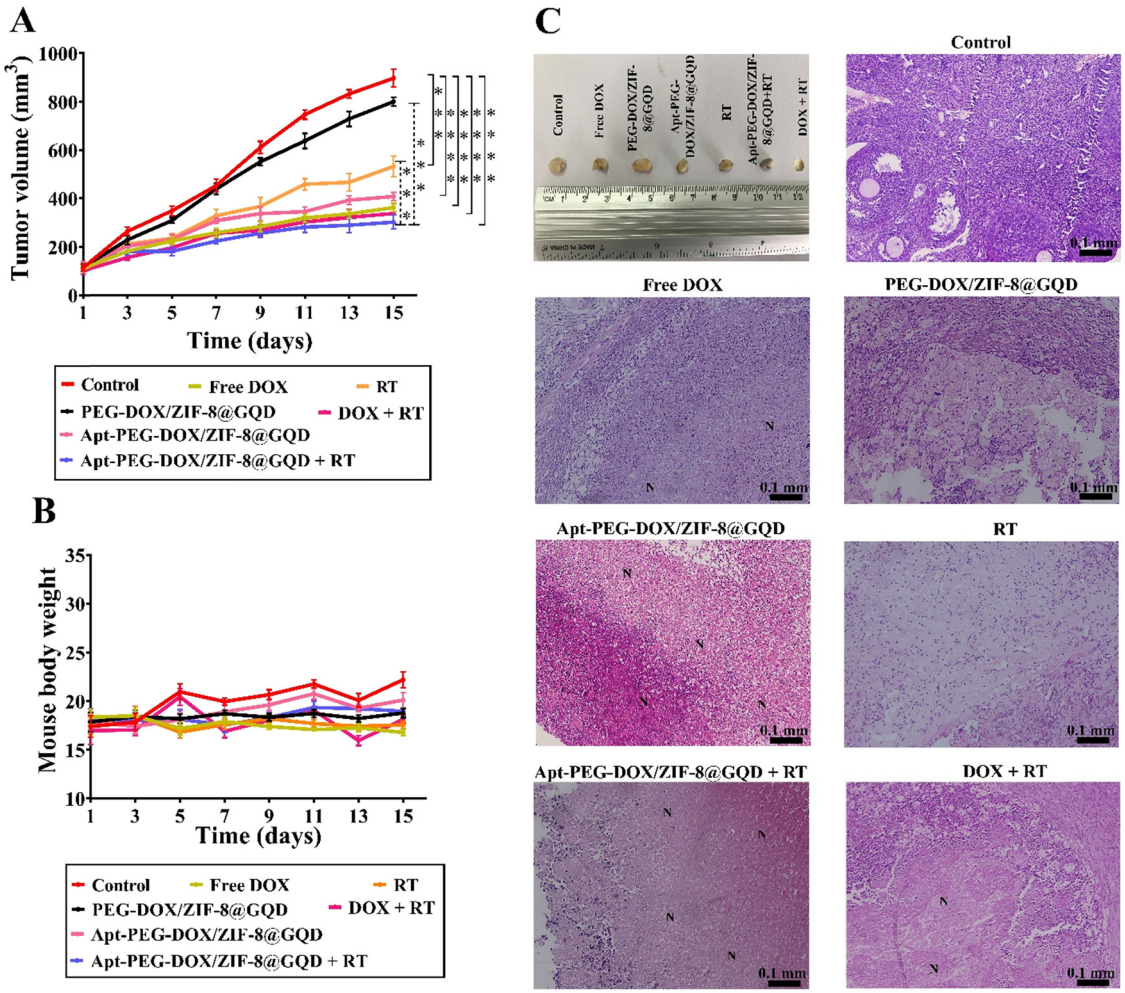


Fig. 6 Comparing the efficacy of mono and combination therapeutic approaches in immunocompromised C57BL/6 mice bearing subcutaneous HT-29 tumors. (A) Tumor growth curves and (B) changes in body weights during 15 days of treatment are plotted. (C) Additionally, representative images of the final dissected tumors from the six experimental groups at the endpoint are presented, along with H&E staining of tumor tissues, indicating cell destruction and the presence of necrotic cells in different groups. "N" denotes necrotic areas within the tumor tissues. Data are presented as mean ± SD; $n = 3$; *** $p < 0.001$ and **** $p < 0.0001$. Scale bars: 0.1 mm. Abbreviations: Gy; gray, Apt; aptamer, PEG; polyethylene glycol, DOX; doxorubicin, ZIF-8; zeolitic imidazolate framework-8, GQD; graphene quantum dot, RT; radiotherapy and SD; standard deviation.

prospect of various formulations (Fig. 7). Histological assessment indicated hepatocyte degeneration and portal area inflammation (yellow arrows) in the liver tissues of free DOX and DOX + RT groups. It should be noted that mild perivascular inflammation (indicated by black arrows) was observed in the lung tissue, and focal areas of infiltration by inflammatory cells (indicated by green arrows) were detected in the heart tissue of the free DOX and DOX + RT groups, respectively. In other treatment groups, no obvious histological abnormalities were observed in the main organs, confirming the advantage of these nano-formulations. The encapsulation of DOX in the nano-delivery systems was found to significantly decrease its adverse side effects. Finally, qualitative and quantitative studies were conducted to assess the tissue distribution of the nano-delivery systems in immunocompromised C57BL/6 mice bearing subcutaneous HT-29 tumors. To accomplish this, various treatment agents were administered intravenously *via* the tail vein, including free DOX, PEG-DOX/ZIF-8@GQD, and Apt-PEG-DOX/ZIF-8@GQD at a dosage of 1 mg $kg^{-1}$ of DOX in 100 μl nanoplatforms. In the combination treatment group, mice were initially administered with Apt-PEG-DOX/ZIF-8@GQD and DOX. After a 4-h interval, the tumors were subjected to a radiation dose of 3 Gy. The major organs and tumors were excised after 12, 24, and 48 h (Fig. 8). In both the free DOX and DOX + RT groups, DOX exhibited non-specific accumulation in the liver, spleen, lung, kidney, heart, and tumor tissues at 12 h. Additionally, the fluorescence intensity of DOX gradually increased in the spleen and lung tissues after 24 h in both treatment groups. PEG-DOX/ZIF-8@GQD was also distributed in main organs and tumor tissue after 12 h and its accumulation in the heart peaked at 24 h. Importantly, the fluorescence intensity of the nano-formulations in the spleen tissue after 12 h was significantly lower than that of free DOX. A significant difference in the fluorescence intensity of Apt-PEG-DOX/ZIF-8@GQD + RT and free DOX in the spleen and heart tissues was observed after 24 h ($p < 0.0001$). More importantly, the intensity of DOX in various animal organs in all treatment groups was decreased after 48 h

 This journal is © The Royal Society of Chemistry 2024

Published on 02 Januari 2024. Downloaded on 19/07/2025 18:32:17.

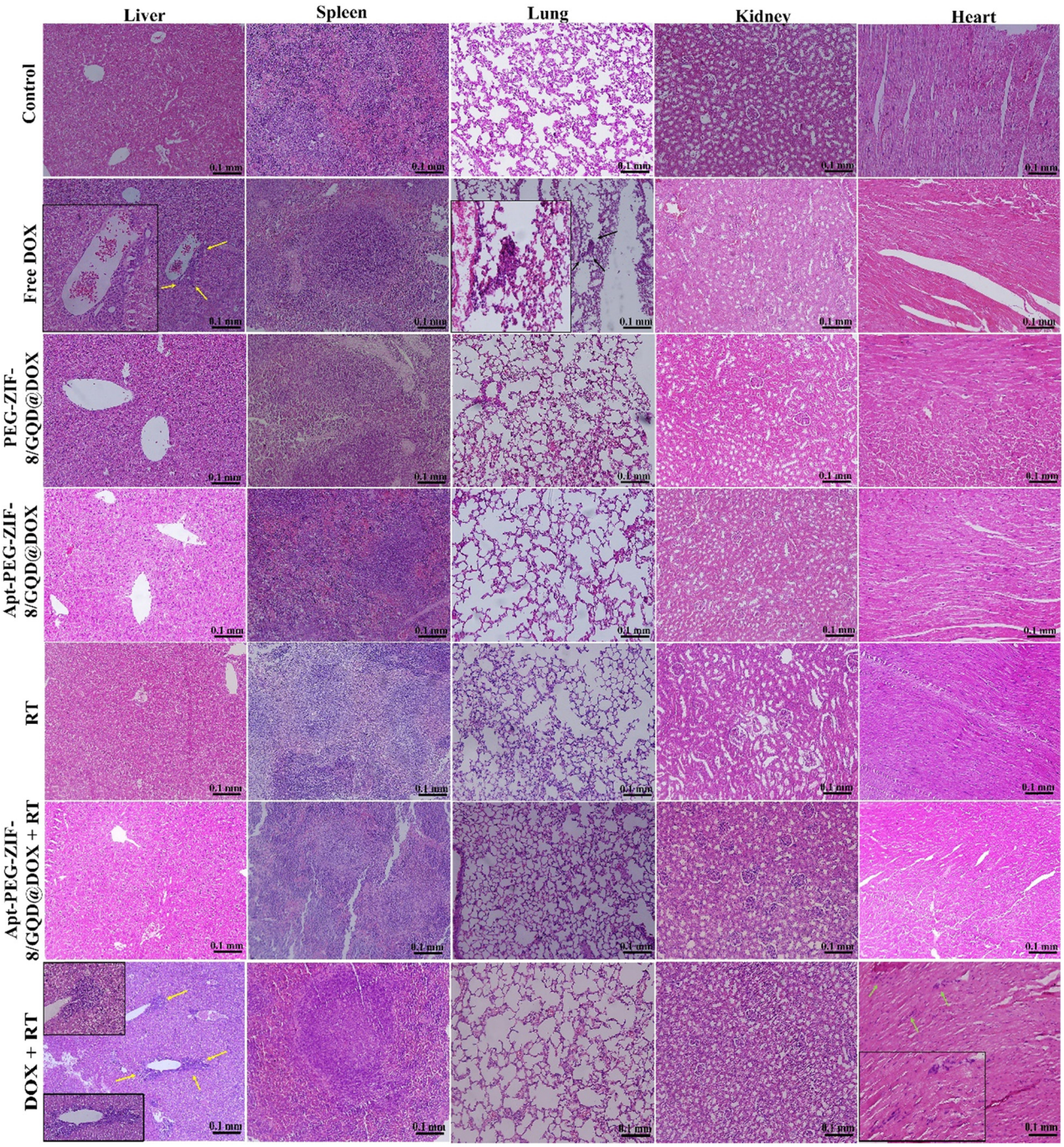


Fig. 7 H&E staining of major organs (liver, spleen, lung, kidney and heart) to evaluate the possible side effects. Hepatocyte degeneration and inflammation in the portal area (indicated by yellow arrows) were observed in the liver tissues of both the free DOX and DOX + RT groups. Additionally, mild perivascular inflammation (indicated by black arrows) was observed in the lung tissue, and a few infiltrating mononuclear inflammatory cells (indicated by green arrows) were detected in the heart tissue of DOX + RT treatment group. Scale bars: 0.1 mm. Abbreviations: H&E; hematoxylin and eosin, Gy; gray, Apt; aptamer, PEG; polyethylene glycol, DOX; doxorubicin, ZIF-8; zeolitic imidazolate framework-8, GQD; graphene quantum dot and RT; radiotherapy.

compared to 12 and 24 h. This disparity could potentially be attributed to the rapid clearance of DOX from the body. In general, free DOX exhibited strong distribution in healthy tissues, leading to systemic toxicity and swift clearance due to its small size, which is consistent with the pathology results. These data provide confirmation that PEGylation could prevent protein binding and prolonged blood circulation, resulting in passive targeting *via* the enhanced permeability and retention (EPR) effect.[72] More importantly, active tumor targeting using the EpCAM aptamer ligand is much faster and more efficient than the passive targeting strategy based on tumor permeation and non-specific distribution. Based on our findings, it is

Published on 02 Januari 2024. Downloaded on 19/07/2025 18:32:17.

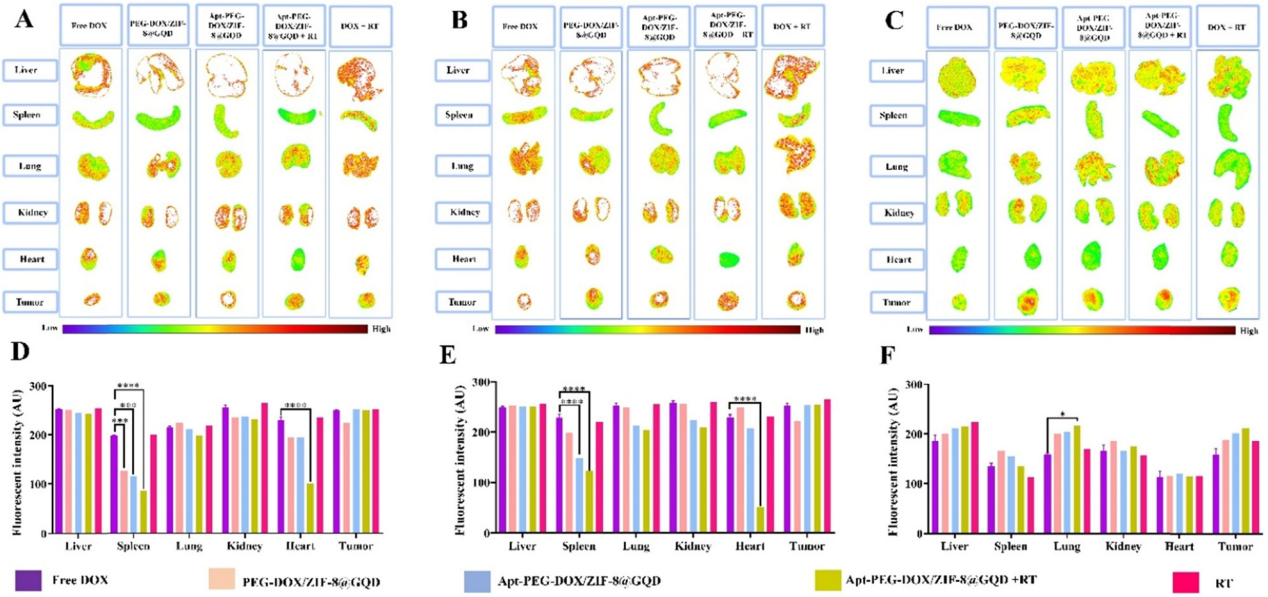


Fig. 8 *In vivo* distribution assessment of nano-delivery systems in C57BL/6 mice bearing HT-29 tumors. *Ex vivo* images of main organs and fluorescence-intensity distribution analysis at (A) and (D) 12 h, (B) and (E) 24 h, and (C) and (F) 48 h post-injection. Intrinsic fluorescence of DOX was used as a signal in IVIS. The values are shown as mean ± SD; $n = 3$, *** $p < 0.001$ and **** $p < 0.0001$. Abbreviations: Gy; gray, Apt; aptamer, PEG; polyethylene glycol, DOX; doxorubicin, ZIF-8; zeolitic imidazolate framework-8, GQD; graphene quantum dot, RT; radiotherapy and IVIS; *in vivo* imaging system.

Table 3 Representative applications of MOFs in combination therapy

| MOFs | Radiosensitizers | Chemotherapy agents | Treatment approaches | Tumor models | Ref. |
|---|---|---|---|---|---|
| Hf-TCPP NMOF-PEG | Hf | None | RT/PDT | 4T1 tumor-bearing mice | 74 |
| BM@NCP(DSP)-PEG | Hf | Cisplatin | RT/Chemotherapy | 4T1 tumor-bearing mice | 75 |
| Mn/Hf-IR825@PDA-PEG | Hf | None | RT/PTT | 4T1 tumor-bearing mice | 76 |
| Hf-BPY-Ir and Hf-BPY-Ru | Hf | None | RT/PDT | CT26 and MC38 tumor-bearing mice | 22 |
| Two Hf- based nMOFs:Hf6-DBA and Hf12-DBA | Hf | Anti-PD-L1 antibody | RT/Immunotherapy | CT26 tumor-bearing mice | 77 |
| DBP-Hf and TBP-Hf | Hf | IDO inhibitor | RT/RDT/Immunotherapy | Different mic models: SQ20B, U87MG, PC-3 and CT26 tumor-bearing mice | 78 |
| Hf- based nMOFs | Hf | Anti-PD-L1 antibody | RT/RDT/Immunotherapy | 4T1 tumor-bearing mice | 70 |
| TB@Hf-BDC-PEG | Hf | TB | RT/Chemotherapy | 4T1 tumor-bearing mice | 79 |
| MnTCPP–Hf–FA MOF | Hf | None | RT | B16-F10 tumor-bearing mice | 80 |
| Zr-MOF-QU | QU | None | RT | A549 tumor-bearing mice | 81 |
| DOX@MOF-Au-PEG | AU | DOX | RT/Chemotherapy | U87MG tumor-bearing mice | 23 |
| Hf-DBB$^F$-Ir and Hf-DBB-Ir | Hf | PAMPs and anti-PD-L1 antibody | RT/RDT/Immunotherapy | MC38 tumor-bearing mice | 82 |
| CBS&DC-ZIF8@DOX | CBS | DOX | RT/Chemotherapy | 4T1 tumor-bearing mice | 83 |
| PEG-Hf-BPY-Fe | Hf | None | RT | HeLa tumor-bearing mice | 84 |
| HA@MIL-100(Fe)/D-Arg | MIL-100(Fe) | D-Arg | RT/Chemotherapy | K7M2 tumor-bearing mice | 73 |
| UiO-66-$NH_2$(Hf) | Hf | None | RT | KYSE-150 tumor-bearing nude mic | 24 |

Abbreviations: Hf; hafnium, TCPP; tetrakis(4-carboxyphenyl)porphyrin, MOFs; metal organic frameworks, PEG; polyethylene glycol, RT; radiotherapy, PDT; photodynamic therapy, DSP; diamminedichlorodisuccinato Pt(IV), PDA; polydopamin, PTT; photo thermal therapy, DBA; 2,5-di(*p*-benzoato)aniline, PD-L1; programmed cell death ligand-1, DBP-Hf; MOFs—5,15-di(*p*-benzoato)porphyrin-Hf, TBP-Hf; 5,10,15,20-tetra(*p*-benzoato)porphyrin-Hf, IDO; immunoregulatory enzyme indoleamine 2,3-dioxygenase, TB; talazoparib and buparlisib, FA; folic acid, QU; quercetin, Au; gold nanoparticle, PAMPs; pathogen-associated molecular patterns, RDT; radio dynamic therapy, CBS; copper bismuth sulfide, HA; hyaluronic acid, and D-Arg; D-arginine.

evident that the utilization of a biocompatible targeted nano-delivery system resulted in significant and specific cytotoxic effects on CRC cells. Furthermore, this nanoplatform served as a well-suited construct for the simultaneous encapsulation of DOX and GQD, enabling multimodal therapy. As a result, this combined treatment approach demonstrated remarkable effectiveness in our experimental setting. Conjugation of radioenhancers with several types of MOFs has been extensively explored, as summarized in

 This journal is © The Royal Society of Chemistry 2024

Published on 02 Januari 2024. Downloaded on 19/07/2025 18:32:17.

Table 3. Du *et al.* showed that the cotreatment with HA@MIL-100(Fe)/D-arginine and RT greatly down-regulated hypoxia-inducible factor-1 alpha (HIF-1α) through nitric oxide production due to the release of D-arginine, thereby preventing lung metastasis in mice-bearing K7M2 cells.[73] Recently, Zhou *et al.* synthesized a nanoscale MOF (UiO-66-$NH_2$(Hf)), which exhibited radiosensitivity in the treatment of esophageal cancer. Their results confirmed the effective tumor inhibition ability after a single intravenous injection of nanoparticles along with a single fraction of X-ray irradiation. As expected, Hf ions could increase the energy deposition in the KYSE-150 tumor-bearing nude mice, leading to complete tumor eradication over 8 days.[24]

## 4. Conclusion

Multimodal cancer therapy, an emerging trend in clinical oncology, involves the use of several treatments to improve the therapeutic index. In this work, we developed a biosafe, pH-sensitive, and efficient nano-vehicle for targeted therapy of CRC using ZIF-8. In this context, the multifunctional nano-delivery system, Apt-PEG-DOX/ZIF-8@GQD, selectively accumulated in the tumor area, co-delivered anti-cancer DOX and GQD radiosensitizer agents, promoted cytotoxicity and effectively enhanced X-ray absorption. The combination of chemo/radio/targeted therapy demonstrated exceptional anti-tumor efficacy in immunocompromised C57BL/6 mice bearing HT-29 human CRC cells. In conclusion, this multifunctional nanocarrier may provide a safe and efficient platform for multimodal cancer therapy.

## Abbreviations

| | |
|---|---|
| AFM | Atomic force microscopy |
| 2-MIM | 2-Methylimidazole |
| BET | Brunauer–Emmett–Teller |
| CFA | Colony formation assay |
| CHO | Chinese hamster ovary |
| CRC | Colorectal cancer |
| DAPI | 4′,6-Diamidino-2-phenylindole |
| DDS | Drug delivery system |
| DMSO | Dimethyl sulfoxide |
| DOX | Doxorubicin |
| ECM | Extracellular matrix |
| EpCAM | Epithelial cell adhesion molecule |
| EPR | Enhanced permeability and retention |
| FE-SEM | Field emission-scanning electron microscopy |
| GQD | Graphene quantum dot |
| Gy | Gray |
| HA | Hyaluronic acid |
| H&E | Hematoxylin & Eosin |
| IR | Ionizing radiation |
| MOF | Metal organic framework |
| OD | Optical density |
| PBS | Phosphate-buffered saline |
| PEG | Polyethylene glycol |
| PE | Plating efficiency |
| PI | Propidium iodide |
| PTT | Photothermal therapy |
| PXRD | Power X-ray diffraction |
| RBC | Red blood cell |
| ROS | Reactive oxygen species |
| RT | Radiotherapy |
| SD | Standard deviation |
| SF | Survival fraction |
| TGA | Thermogravimetric analysis |
| TEM | Transmission electron microscopy |
| TME | Tumor microenvironment |
| ZIF-8 | Zeolitic imidazolate framework-8 |

## Availability of data and materials

The datasets used and/or analyzed during the current study are available from the corresponding authors on reasonable request.

## Authors' contributions

SI: conducted the methodology and inferences, carried out statistical analyses, and wrote the manuscript. ARB: advisor, provided financial support, analyzed the results, and proofread the manuscript. MD: advisor, proofread the manuscript and carried out radiotherapy. ASS: supervisor, conceived the original idea and designed the study, provided financial support, analyzed the results, and wrote the manuscript. MMM: supervisor, conceived the original idea and designed the study, provided financial support, analyzed the results, and wrote the manuscript. All authors read and approved the final manuscript.

## Conflicts of interest

The authors declare that there is no conflict of interest.

## Acknowledgements

The authors would like to thank Mr Khalili-Hezarjaribi, Mr Malaekeh, Dr Noroozpour and Dr Shaterzade for their excellent support and technical assistance. We are also grateful to the Reza Radiotherapy and Oncology Center for their technical help. This work was supported by Ferdowsi University of Mashhad, grant number: 3.51537.

## References

1 T. Sawicki, *et al.*, A review of colorectal cancer in terms of epidemiology, risk factors, development, symptoms and diagnosis, *Cancers*, 2021, **13**(9), 2025.
2 Y. Xi and P. Xu, Global colorectal cancer burden in 2020 and projections to 2040, *Transl. Oncol.*, 2021, **14**(10), 101174.
3 M. U. R. Naidu, *et al.*, Chemotherapy-induced and/or radiation therapy-induced oral mucositis-complicating the treatment of cancer, *Neoplasia*, 2004, **6**(5), 423–431.

Published on 02 Januari 2024. Downloaded on 19/07/2025 18:32:17.

4 H. Kato, *et al.*, Evaluation of the Efficacy of Doxorubicin against Gastrointestinal Cancer, *Ann. Oncol.*, 2012, **23**, xi160.
5 N. Potočnik, *et al.*, Cardiac autonomic modulation induced by doxorubicin in a rodent model of colorectal cancer and the influence of fullerenol pretreatment, *PLoS One*, 2017, **12**(7), e0181632.
6 X. Y. Zhang and P. Y. Zhang, Nanotechnology for multimodality treatment of cancer, *Oncol. Lett.*, 2016, **12**(6), 4883–4886.
7 S. Iranpour, *et al.*, Application of smart nanoparticles as a potential platform for effective colorectal cancer therapy, *Coord. Chem. Rev.*, 2021, **442**, 213949.
8 S. Feng, *et al.*, Zeolitic imidazolate framework-8 (ZIF-8) for drug delivery: A critical review, *Front. Chem. Sci. Eng.*, 2021, **15**(2), 221–237.
9 M. Saeinasab, *et al.*, Tumor-targeted delivery of *SNHG15* siRNA using a ZIF-8 nanoplatform: Towards a more effective prostate cancer therapy, *Int. J. Biol. Macromol.*, 2024, **259**, 129233, DOI: **10.1016/j.ijbiomac.2024.129233**.
10 L. Gong, *et al.*, Application of radiosensitizers in cancer radiotherapy, *Int. J. Nanomed.*, 2021, **16**, 1083.
11 J. Ruan, *et al.*, Graphene quantum dots for radiotherapy, *ACS Appl. Mater. Interfaces*, 2018, **10**(17), 14342–14355.
12 S. Iravani and R. S. Varma, Green synthesis, biomedical and biotechnological applications of carbon and graphene quantum dots. A review, *Environ. Chem. Lett.*, 2020, **18**(3), 703–727.
13 Y. Chong, *et al.*, The in vitro and *in vivo* toxicity of graphene quantum dots, *Biomaterials*, 2014, **35**(19), 5041–5048.
14 G. L. Hong, *et al.*, Fabrication of ultra-small monolayer graphene quantum dots by pyrolysis of trisodium citrate for fluorescent cell imaging, *Int. J. Nanomed.*, 2018, **13**, 4807.
15 T. A. Tabish, *et al.*, Biocompatibility and toxicity of graphene quantum dots for potential application in photodynamic therapy, *Nanomedicine*, 2018, **13**(15), 1923–1937.
16 R. Sekiya, *et al.*, White-light-emitting edge-functionalized graphene quantum dots, *Angew. Chem.*, 2014, **126**(22), 5725–5729.
17 M. Thakur, M. K. Kumawat and R. Srivastava, Multifunctional graphene quantum dots for combined photothermal and photodynamic therapy coupled with cancer cell tracking applications, *RSC Adv.*, 2017, **7**(9), 5251–5261.
18 H. Liu, *et al.*, Magnetic-induced graphene quantum dots for imaging-guided photothermal therapy in the second near-infrared window, *Biomaterials*, 2020, **232**, 119700.
19 X. Yuan, *et al.*, Cellular distribution and cytotoxicity of graphene quantum dots with different functional groups, *Nanoscale Res. Lett.*, 2014, **9**(1), 1–9.
20 Y. Zhou, *et al.*, How functional groups influence the ROS generation and cytotoxicity of graphene quantum dots, *Chem. Commun.*, 2017, **53**(76), 10588–10591.
21 Z. Tian, *et al.*, Metal–organic framework/graphene quantum dot nanoparticles used for synergistic chemo-and photothermal therapy, *ACS Omega*, 2017, **2**(3), 1249–1258.
22 G. Lan, *et al.*, Nanoscale metal–organic layers for deeply penetrating X-ray-induced photodynamic therapy, *Angew. Chem.*, 2017, **129**(40), 12270–12274.
23 Z. He, *et al.*, A Catalase-Like Metal-Organic Framework Nanohybrid for $O_2$-Evolving Synergistic Chemoradiotherapy, *Angew. Chem.*, 2019, **131**(26), 8844–8848.
24 W. Zhou, *et al.*, Hafnium-Based Metal–Organic Framework Nanoparticles as a Radiosensitizer to Improve Radiotherapy Efficacy in Esophageal Cancer, *ACS Omega*, 2022, **7**(14), 12021–12029.
25 M. F. Attia, *et al.*, An overview of active and passive targeting strategies to improve the nanocarriers efficiency to tumour sites, *J. Pharm. Pharmacol.*, 2019, **71**(8), 1185–1198.
26 L. S. Boogerd, *et al.*, Biomarker expression in rectal cancer tissue before and after neoadjuvant therapy, *OncoTargets Ther.*, 2018, **11**, 1655.
27 K. M. Song, S. Lee and C. Ban, Aptamers and their biological applications, *Sensors*, 2012, **12**(1), 612–631.
28 Q. Zhu, G. Liu and M. Kai, DNA aptamers in the diagnosis and treatment of human diseases, *Molecules*, 2015, **20**(12), 20979–20997.
29 S. Iranpour, *et al.*, Improving anti-cancer drug delivery performance of magnetic mesoporous silica nanocarriers for more efficient colorectal cancer therapy, *J. Nanobiotechnol.*, 2021, **19**(1), 1–22.
30 Y. Song, *et al.*, Selection of DNA aptamers against epithelial cell adhesion molecule for cancer cell imaging and circulating tumor cell capture, *Anal. Chem.*, 2013, **85**(8), 4141–4149.
31 H. Zheng, *et al.*, One-pot synthesis of metal–organic frameworks with encapsulated target molecules and their applications for controlled drug delivery, *J. Am. Chem. Soc.*, 2016, **138**(3), 962–968.
32 J. Bi, *et al.*, Synthesis of Folic Acid-Modified DOX@ZIF-8 Nanoparticles for Targeted Therapy of Liver Cancer, *J. Nanomater.*, 2018, **2018**, 1357812.
33 M. Wu, *et al.*, A poly (ethylenglycol) functionalized ZIF-8 membrane prepared by coordination-based post-synthetic strategy for the enhanced adsorption of phenolic endocrine disruptors from water, *Sci. Rep.*, 2017, **7**(1), 1–11.
34 Q. Yu, *et al.*, Poly (ethylene glycol)-mediated mineralization of metal–organic frameworks, *Chem. Commun.*, 2020, **56**(75), 11078–11081.
35 Y. Hazeri, *et al.*, Dual-targeted delivery of doxorubicin by mesoporous silica nanoparticle coated with AS1411 aptamer and RGDK-R peptide to breast cancer in vitro and *in vivo*, *J. Drug Delivery Sci. Technol.*, 2022, **71**, 103285.
36 C. Y. Sun, *et al.*, Zeolitic imidazolate framework-8 as efficient pH-sensitive drug delivery vehicle, *Dalton Trans.*, 2012, **41**(23), 6906–6909.
37 L. He, *et al.*, Carbon nanodots@ zeolitic imidazolate framework-8 nanoparticles for simultaneous pH-responsive drug delivery and fluorescence imaging, *CrystEngComm*, 2014, **16**(16), 3259–3263.
38 M. A. Dobrovolskaia, *et al.*, Method for analysis of nanoparticle hemolytic properties in vitro, *Nano Lett.*, 2008, **8**(8), 2180–2187.
39 C. Lee, *et al.*, Ultrasmall Gd@ Cdots as a radiosensitizing agent for non-small cell lung cancer, *Nanoscale*, 2021, **13**(20), 9252–9263.
40 S. Iranpour, *et al.*, Investigating the effects of two novel 4-MMPB analogs as potent lipoxygenase inhibitors for prostate cancer treatment, *J. Biol. Res.*, 2021, **28**(1), 1–15.

 This journal is © The Royal Society of Chemistry 2024

Published on 02 Januari 2024. Downloaded on 19/07/2025 18:32:17.

41 K. Habiba, *et al.*, Enhancing colorectal cancer radiation therapy efficacy using silver nanoprisms decorated with graphene as radiosensitizers, *Sci. Rep.*, 2019, **9**(1), 1–9.
42 M. Adnan, *et al.*, X-shaped ZIF-8 for immobilization rhizomucor miehei lipase via encapsulation and its application toward biodiesel production, *Catalysts*, 2018, **8**(3), 1–14.
43 B. P. Biswal, *et al.*, Stabilization of graphene quantum dots (GQDs) by encapsulation inside zeolitic imidazolate framework nanocrystals for photoluminescence tuning, *Nanoscale*, 2013, **5**(21), 10556–10561.
44 B. Chen, Y. Zhu and Y. Xia, Controlled in situ synthesis of graphene oxide/zeolitic imidazolate framework composites with enhanced $CO_2$ uptake capacity, *RSC Adv.*, 2015, **5**(39), 30464–30471.
45 D. Pan, *et al.*, Synthesis of graphene quantum dot/metal–organic framework nanocomposites as yellow phosphors for white light-emitting diodes, *New J. Chem.*, 2018, **42**(7), 5083–5089.
46 H. Hayashi, *et al.*, Zeolite A imidazolate frameworks, *Nat. Mater.*, 2007, **6**(7), 501–506.
47 X. Feng, *et al.*, MXene quantum dot/zeolitic imidazolate framework nanocarriers for dual stimulus triggered tumor chemo-phototherapy, *Materials*, 2022, **15**(13), 4543.
48 X. Mi, *et al.*, Folic acid decorated zeolitic imidazolate framework (ZIF-8) loaded with baicalin as a nano-drug delivery system for breast cancer therapy, *Int. J. Nanomed.*, 2021, **16**, 8337.
49 H. Kaur, *et al.*, Synthesis and characterization of ZIF-8 nanoparticles for controlled release of 6-mercaptopurine drug, *J. Drug Delivery Sci. Technol.*, 2017, **41**, 106–112.
50 H. Xiao and L. Wang, Effects of X-shaped reduction-sensitive amphiphilic block copolymer on drug delivery, *Int. J. Nanomed.*, 2015, **10**, 5309.
51 H. Wang, *et al.*, One-pot synthesis of poly(ethylene glycol) modified zeolitic imidazolate framework-8 nanoparticles: Size control, surface modification and drug encapsulation, *Colloids Surf., A*, 2019, **568**, 224–230.
52 H. Guo, *et al.*, Monodisperse ZIF-8@ dextran nanoparticles co-loaded with hydrophilic and hydrophobic functional cargos for combined near-infrared fluorescence imaging and photothermal therapy, *Acta Biomater.*, 2022, **137**, 290–304.
53 B. Liu, *et al.*, Real-time drug release monitoring from pH-responsive CuS-encapsulated metal–organic frameworks, *RSC Adv.*, 2022, **12**(18), 11119–11127.
54 A. S. Spitsyna, *et al.*, Stability of ZIF-8 nanoparticles in most common cell culture media, *Molecules*, 2022, **27**(10), 3240.
55 A. G. Niculescu and A. M. Grumezescu, Novel tumor-targeting nanoparticles for cancer treatment—A review, *Int. J. Mol. Sci.*, 2022, **23**(9), 5253.
56 D. Venturoli and B. Rippe, Ficoll and dextran vs. globular proteins as probes for testing glomerular permselectivity: effects of molecular size, shape, charge, and deformability, *Am. J. Physiol.: Renal Physiol.*, 2005, **288**(4), F605–F613.
57 Z. Hussain, *et al.*, PEGylation: A promising strategy to overcome challenges to cancer-targeted nanomedicines: A review of challenges to clinical transition and promising resolution, *Drug Delivery Transl. Res.*, 2019, **9**(3), 721–734.
58 J. Lin, *et al.*, Effects of ZIF-8 MOFs on structure and function of blood components, *RSC Adv.*, 2021, **11**(35), 21414–21425.
59 S. Astm, Standard practice for assessment of hemolytic properties of materials, Annual Book of ASTM Standards, Committee F04 Medical and Surgical Materials and Devices, Subcommittee F04.16 Biocompatibility Test Methods. Annual Book of ASTM Standards, 2009. Astm.[Google Scholar], 2008.
60 Q.-g Zhao, *et al.*, A ZnO-gated porphyrinic metal–organic framework-based drug delivery system for targeted bimodal cancer therapy, *J. Mater. Chem. B*, 2018, **6**(47), 7898–7907.
61 Q. Sun, *et al.*, Hyaluronic acid-targeted and pH-responsive drug delivery system based on metal-organic frameworks for efficient antitumor therapy, *Biomaterials*, 2019, **223**, 119473.
62 D. Hallahan, *et al.*, Targeting drug delivery to radiation-induced neoantigens in tumor microvasculature, *J. Controlled Release*, 2001, **74**(1–3), 183–191.
63 D. Hallahan, *et al.*, Integrin-mediated targeting of drug delivery to irradiated tumor blood vessels, *Cancer Cell*, 2003, **3**(1), 63–74.
64 T. Lammers, *et al.*, Image-guided and passively tumour-targeted polymeric nanomedicines for radiochemotherapy, *Br. J. Cancer*, 2008, **99**(6), 900–910.
65 S. Stapleton, D. Jaffray and M. Milosevic, Radiation effects on the tumor microenvironment: Implications for nanomedicine delivery, *Adv. Drug Delivery Rev.*, 2017, **109**, 119–130.
66 K. J. Lee, *et al.*, A strategy for actualization of active targeting nanomedicine practically functioning in a living body, *Biomaterials*, 2017, **141**, 136–148.
67 X. Yi, *et al.*, Biomimetic copper sulfide for chemo-radiotherapy: enhanced uptake and reduced efflux of nanoparticles for tumor cells under ionizing radiation, *Adv. Funct. Mater.*, 2018, **28**(9), 1705161.
68 M. A. Miller, *et al.*, Radiation therapy primes tumors for nanotherapeutic delivery via macrophage-mediated vascular bursts, *Sci. Transl. Med.*, 2017, **9**(392), eaal0225.
69 G. Erel-Akbaba, *et al.*, Radiation-induced targeted nanoparticle-based gene delivery for brain tumor therapy, *ACS Nano*, 2019, **13**(4), 4028–4040.
70 K. Ni, *et al.*, Ultrathin metal-organic-layer mediated radiotherapy-radiodynamic therapy, *Matter*, 2019, **1**(5), 1331–1353.
71 J. Yu, *et al.*, Peptide-modified bioresponsive chondroitin sulfate micelles for targeted doxorubicin delivery in triple-negative breast cancer, *Colloids Surf., B*, 2023, **227**, 113381.
72 S. Hua, *et al.*, Multistage-responsive clustered nanosystem to improve tumor accumulation and penetration for photothermal/enhanced radiation synergistic therapy, *Biomaterials*, 2021, **268**, 120590.
73 C. Du, *et al.*, D-arginine-loaded metal-organic frameworks nanoparticles sensitize osteosarcoma to radiotherapy, *Biomaterials*, 2021, **269**, 120642.
74 J. Liu, *et al.*, Nanoscale metal– organic frameworks for combined photodynamic & radiation therapy in cancer treatment, *Biomaterials*, 2016, **97**, 1–9.

Published on 02 Januari 2024. Downloaded on 19/07/2025 18:32:17.

75 J. Liu, *et al.*, Nanoscale-coordination-polymer-shelled manganese dioxide composite nanoparticles: A multistage redox/pH/$H_2O_2$-responsive cancer theranostic nanoplatform, *Adv. Funct. Mater.*, 2017, **27**(10), 1605926.
76 Y. Yang, *et al.*, Core-shell and co-doped nanoscale metal-organic particles (NMOPs) obtained via post-synthesis cation exchange for multimodal imaging and synergistic thermo-radiotherapy. NPG Asia, *Materials*, 2017, **9**(1), e344.
77 K. Ni, *et al.*, Nanoscale metal-organic frameworks enhance radiotherapy to potentiate checkpoint blockade immunotherapy, *Nat. Commun.*, 2018, **9**(1), 1–12.
78 K. Lu, *et al.*, Low-dose X-ray radiotherapy–radiodynamic therapy via nanoscale metal–organic frameworks enhances checkpoint blockade immunotherapy, *Nat. Biomed. Eng.*, 2018, **2**(8), 600–610.
79 M. J. Neufeld, *et al.*, Co-delivery of PARP and PI3K inhibitors by nanoscale metal–organic frameworks for enhanced tumor chemoradiation, *Nano Res.*, 2019, **12**(12), 3003–3017.
80 Y. Chen, *et al.*, Catalase-like metal–organic framework nanoparticles to enhance radiotherapy in hypoxic cancer and prevent cancer recurrence, *Chem. Sci.*, 2019, **10**(22), 5773–5778.
81 T. Ma, *et al.*, Quercetin-modified metal–organic frameworks for dual sensitization of radiotherapy in tumor tissues by inhibiting the carbonic anhydrase IX, *ACS Nano*, 2019, **13**(4), 4209–4219.
82 K. Ni, *et al.*, Nanoscale metal-organic frameworks for X-ray activated in situ cancer vaccination, *Sci. Adv.*, 2020, **6**(40), eabb5223.
83 Y. Kang, *et al.*, Tetramodal imaging and synergistic cancer radio-chemotherapy enabled by multiple component-encapsulated zeolitic imidazolate frameworks, *ACS Nano*, 2020, **14**(4), 4336–4351.
84 T. Gong, *et al.*, Full-process radiosensitization based on nanoscale metal–organic frameworks, *ACS Nano*, 2020, **14**(3), 3032–3040.

 This journal is © The Royal Society of Chemistry 2024